Mathematics, Physics, and Computer Science
Faculty Articles and Research

Science and Technology Faculty Articles and
Research

2014

Effects of Crop Residue Burning on Aerosol Properties, Plume Characteristics, and Long-Range Transport over Northern India

D. G. Kaskaoutis
Shiv Nadar University, India

S. Kumar
Banaras Hindu University, India

D. Sharma
Punjabi University, India

Ramesh P. Singh
Chapman University, rsingh@chapman.edu

S. K. Kharol
Dalhousie University, Canada

See next page for additional authors

Follow this and additional works at: https://digitalcommons.chapman.edu/scs_articles

Part of the Atmospheric Sciences Commons, Environmental Health and Protection Commons, and the Environmental Indicators and Impact Assessment Commons

Recommended Citation

Effects of Crop Residue Burning on Aerosol Properties, Plume Characteristics, and Long-Range Transport over Northern India

Authors

D. G. Kaskaoutis, S. Kumar, D. Sharma, Ramesh P. Singh, S. K. Kharol, M. Sharma, A. K. Singh, Atinderpal Singh, and D. Singh

Correspondence to:
R. P. Singh,
rsingh@chapman.edu

Effects of crop residue burning on aerosol properties, plume characteristics, and long-range transport over northern India

D. G. Kaskaoutis[1], S. Kumar[2], D. Sharma[3], R. P. Singh[4], S. K. Kharol[5], M. Sharma[6], A. K. Singh[2], S. Singh[7], Atinderpal Singh[3], and D. Singh[3]

[1]Department of Physics, School of Natural Sciences, Shiv Nadar University, Tehsil Dadri, India, [2]Atmospheric Research Laboratory, Department of Physics, Banaras Hindu University, Varanasi, India, [3]Physics Department, Punjabi University, Patiala, India, [4]School of Earth and Environmental Sciences, Schmid College of Science and Technology, Chapman University, Orange, California, USA, [5]Department of Physics and Atmospheric Science, Dalhousie University, Halifax, Nova Scotia, Canada, [6]Research and Technology Development Centre, Sharda University, Greater Noida, India, [7]Radio and Atmospheric Sciences Division, National Physical Laboratory, New Delhi, India

Abstract Aerosol emissions from biomass burning are of specific interest over the globe due to their strong radiative impacts and climate implications. The present study examines the impact of paddy crop residue burning over northern India during the postmonsoon (October–November) season of 2012 on modification of aerosol properties, as well as the long-range transport of smoke plumes, altitude characteristics, and affected areas via the synergy of ground-based measurements and satellite observations. During this period, Moderate Resolution Imaging Spectroradiometer (MODIS) images show a thick smoke/hazy aerosol layer below 2–2.5 km in the atmosphere covering nearly the whole Indo-Gangetic Plains (IGP). The air mass trajectories originating from the biomass-burning source region over Punjab at 500 m reveal a potential aerosol transport pathway along the Ganges valley from west to east, resulting in a strong aerosol optical depth (AOD) gradient. Sometimes, depending upon the wind direction and meteorological conditions, the plumes also influence central India, the Arabian Sea, and the Bay of Bengal, thus contributing to Asian pollution outflow. The increased number of fire counts (Terra and Aqua MODIS data) is associated with severe aerosol-laden atmospheres ($AOD_{500\,nm} > 1.0$) over six IGP locations, high values of Ångström exponent (>1.2), high particulate mass 2.5 ($PM_{2.5}$) concentrations (>100–$150\,\mu gm^{-3}$), and enhanced Ozone Monitoring Instrument Aerosol Index gradient (~2.5) and NO_2 concentrations (~6×10^{15} mol/cm^2), indicating the dominance of smoke aerosols from agricultural crop residue burning. The aerosol size distribution is shifted toward the fine-mode fraction, also exhibiting an increase in the radius of fine aerosols due to coagulation processes in a highly turbid environment. The spectral variation of the single-scattering albedo reveals enhanced dominance of moderately absorbing aerosols, while the aerosol properties, modification, and mixing atmospheric processes differentiate along the IGP sites depending on the distance from the aerosol source, urban influence, and local characteristics.

1. Introduction

Biomass burning is a common source of atmospheric pollution and poor air quality that has adverse impacts at local, regional, and global scales with direct short- and long-term climate implications and serious risk to human health [*Andreae and Merlet*, 2001; *Arola et al.*, 2007; *Nastos et al.*, 2010]. On a global scale, the contribution of biomass-burning aerosols to radiative forcing was found to be $+0.04 \pm 0.07\,W\,m^{-2}$ [*Forster et al.*, 2007], thereby reducing the amount of sunlight reaching the Earth's surface and heating the lower and middle troposphere. Furthermore, the radiative effect of smoke must be taken into account to predict the overall impact of aerosols on local weather and regional climate that alters atmospheric dynamics and thermodynamics [*Turetsky et al.*, 2011]. On a global scale, the burning of agricultural crop residue and clearing of forests accounts for about 90% of total wildfires [*Food and Agriculture Organization*, 2009; *Barnaba et al.*, 2011] mostly occurring in equatorial and South Africa, Amazonia, and Southeast Asia; the remaining 10% is dominated by wild forest fires and grassland burning.

Local and regional meteorology (air temperature, wind speed, and prolonged droughts) plays a crucial role in the ignition and spread of forest fires, while agricultural burning is commonly practiced by the farmers in developing countries to improve the nutrition level in the soil and agricultural productivity. In Asia, three types

of burning activities dominate, (i) forest fires (45%), (ii) agricultural crop residue burning (34%), and (iii) grassland fires (20%), with India exhibiting the second highest crop residue burning (84 Tg/yr) [*Streets and Yarber*, 2003]. It was estimated that rice residue produced in India is ~97 Tg (6 years 1999–2005 average) out of which 22–23% is usually burned in fields as surplus, producing huge amounts of carbonaceous aerosols and trace gases [*Gadde et al.*, 2009; *Vadrevu et al.*, 2011].

Aerosols over India show a mixture of anthropogenic emissions, smoke from seasonal forest fires or crop residue burning, long-range transported or even locally produced dust, and particles of marine origin during the summer monsoon. Every year, during the postmonsoon season (October–November), extensive agricultural (rice) crop residue burning takes place in the Indo-Gangetic Plains (IGP), mainly in the northwestern Indian states of Punjab, Haryana, and western Uttar Pradesh [*Sarkar et al.*, 2013]. The emissions from the burning locations travel thousands of kilometers downwind, covering the IGP from west to east. Sometimes, depending on the wind speed and direction; the Arabian Sea and central south India are also affected [*Badarinath et al.*, 2009a, 2009b]. The mostly absorbing biomass-burning aerosols contribute significantly to the surface radiative forcing (-57.2 to $-96.9\,\mathrm{W\,m^{-2}}$) over the region and are responsible for large (43.0 to 86.5 $\mathrm{W\,m^{-2}}$) atmospheric (lower and middle troposphere) heating [*Sharma et al.*, 2012]. Internal or external mixing with other anthropogenic and natural aerosols forms the Atmospheric Brown Clouds, composed of soot, sulfates, organics, dust, etc. [*Carimichael et al.*, 2009], that contribute to the Asian pollution outflow and haze [*Lawrence and Lelieveld*, 2010], which plays an important role in solar dimming, atmospheric heating and stability, monsoon circulation, and hydrological cycle [*Pinker et al.*, 2005; *Ramanathan et al.*, 2005, 2007; *Tripathi et al.*, 2007; *Bollasina et al.*, 2008; *Randles and Ramaswamy*, 2008]. Furthermore, *Gustafsson et al.* [2009] observed that black carbon (BC) aerosols and associated dense brown clouds affect human health, cause pulmonary disease, bronchitis, and asthma. Depending on the nature of the biomass-burning conditions, biomass-burning aerosols exhibit different optical properties in how they absorb, reflect, and scatter solar radiation [*Reid et al.*, 1999; *Eck et al.*, 2003]. As a consequence, they induce an increase or reduction of cloud cover and albedo, depending on the vertical distribution of the aerosols within or above the clouds [*Feingold et al.*, 2005] and reduce rainfall [*Rosenfeld*, 2000]. However, the interaction between biomass-burning aerosols and clouds, either over land or the oceans, is a highly complicated and uncertain phenomenon strongly dependent on the vertical distribution and relative height between absorbing aerosols and clouds [*Koch and Del Genio*, 2010]. In view of the important role of biomass burning over the IGP, the quantitative evaluation of aerosol loading, emission characteristics, and long-range smoke plume transport has to be examined.

Satellite remote sensing is a well-established tool for monitoring wildfires, mapping the burned areas, and evaluating biomass-burning aerosols [*Kahn et al.*, 2007; *Kaskaoutis et al.*, 2011a; *Barnaba et al.*, 2011; *Gautam et al.*, 2013]. The NASA Moderate Resolution Imaging Spectroradiometer (MODIS) sensor includes a 1 km active fire product (http://rapidfire.sci.gsfc.nasa.gov/) and a burned area product at 500 m resolution [*Giglio et al.*, 2003; *Roy et al.*, 2005]. Furthermore, in situ campaigns (Smoke Clouds, and Radiation-Brazil, Southern African Fire-Atmosphere Research Initiative, and Zambian International Biomass Burning Emissions Experiment) have taken place at several areas over the globe suffering from seasonal forest fires and biomass burning [*Reid et al.*, 1999; *Eck et al.*, 2001, 2003]. In recent years, several techniques have been established for satellite monitoring of forest fires, also associated with chemical transport models simulating smoke plumes and their impact from local-to-regional scales [*Kontoes et al.*, 2009; *Hodnebrog et al.*, 2012; *Reche et al.*, 2012].

The present study mainly focuses on investigating the effects of extensive crop residue burning during the postmonsoon season of 2012 on the modification of aerosol properties over northern India and studying the altitude variation of smoke plumes and the regions that are mostly affected. In this respect, a synergy of ground-based (Sun photometer measurements at six locations over the IGP) and satellite observations (MODIS, Ozone Monitoring Instrument (OMI), and CALIPSO) was utilized. Initially, temporal and spatial evolution of the fire counts and associated aerosol emissions via MODIS and OMI sensors is studied over the IGP during October–November 2012. In the second part, analysis of the trajectory altitudes and the downwind-affected areas takes place. Furthermore, Sun photometer (Microtops-II and CIMEL) measurements of several aerosol properties over six IGP sites are utilized to study the effects of agricultural biomass burning.

Table 1. Locations, Instruments, and Availability of Data in the Indo-Gangetic Plains Used in the Current Study During the Postmonsoon (October–November) Season of 2012

Location	Instruments	Availability of Measurements
Patiala (30.33°N, 76.40°E, 249 m)	Microtops-II Sun photometer; six channels (380, 440, 500, 675, 800, and 870 nm)/GRIMM	44 days, 700 scans/PM_{10}, $PM_{2.5}$, and $PM_{1.0}$ (daily: 09:00–16:00 LT)
Delhi (28.38°N, 77.08°E, 238 m)	Microtops-II Sun photometer; four channels (340, 500, 870, and 1020 nm)	27 days, 254 scans
Greater Noida (28.28°N, 77.28°E, 248 m)	Microtops-II Sun photometer; five channels (440, 500, 675, 870, and 936 nm)	32 days, 64 scans
Kanpur (26.51°N, 80.23°E, 123 m)	AERONET CIMEL 318; seven channels (340, 380, 440, 500, 675, 870, and 1020 nm)	51 days, 1779 scans
Varanasi (25.27°N, 82.99°E, 83 m)	Microtops-II Sun photometer; five channels (380, 440, 500, 675, and 870 nm)	53 days, 813 scans
Gandhi College (25.87°N, 84.12°E, 60 m)	AERONET CIMEL 318; seven channels (340, 380, 440, 500, 675, 870, and 1020 nm)	57 days, 1567 scans

2. Material and Methods

2.1. Study Region

The state of Punjab in northwestern India produces about two thirds of the country's food grains and is known as the country's "bread basket" [*Sharma et al.*, 2010]. This region, as well as the nearby states of Haryana and Uttar Pradesh, is dominated by annual wheat-rice crop rotation, and the harvesting leaves large quantities of straw in the fields. The wheat residue is usually used for animal feed, but the paddy residue is burnt (~17×10^6 t each year) in the fields, emitting large amounts of submicron aerosols and trace gases (CO_2, CO, CH_4, N_2O, SO_2, NO_x, and nonmethane hydrocarbons) [*Sahai et al.*, 2007]. During the postmonsoon season (October–November), weather over the IGP is fairly dry with average daytime relative humidity in the range of 40–70%, moderate temperatures of 20–30°C and light winds (1–2 m s^{-1}) from the northwest, favoring the accumulation of aerosols and their slow transport along the Ganges valley [*Mishra and Shibata*, 2012]. The postmonsoon seasons of 2006 and 2007 have already been analyzed [*Badarinath et al.*, 2009a, 2009b; *Sharma et al.*, 2010], as well as the severe aerosol-laden atmospheres in 2008 [*Kharol et al.*, 2012; *Sharma et al.*, 2012]. Furthermore, *Mishra and Shibata* [2012] performed a comprehensive analysis of aerosol optical properties and vertical profiles over the IGP during postmonsoon 2009. The present study emphasizes the intense biomass-burning season of postmonsoon 2012, when thick smoke plumes covered the whole IGP region for many days.

2.2. Data Set

Multiple ground-based and satellite observations of various aerosol properties have been carried out over the IGP during the postmonsoon 2012. The season is divided into four subperiods based on the number of fire counts, the intensity of the agricultural burning, the associated emissions and aerosol loading, i.e., (i) preburning (1–15 October 2012), (ii) early burning (15–30 October 2012), (iii) late burning (1–17 November 2012), and (iv) postburning (18–30 November 2012).

2.2.1. Microtops-II Sun Photometer

Table 1 summarizes the ground-based data set used in the present study corresponding mostly to Sun photometer measurements over six IGP sites, from northwest (Patiala) to southeast (Gandhi College) (Figure 1). At four locations (Patiala, Delhi, Greater Noida, and Varanasi), the spectral aerosol optical depth (AOD) measurements were taken by means of Microtops-II (MT) Sun photometer at various wavelength channels, while in Kanpur and Gandhi College, the data set consists of AERONET (Aerosol Robotic Network) recordings. MT Sun photometers have been extensively used for aerosol studies over Patiala [*Kharol et al.*, 2012; *Sharma et al.*, 2012], Delhi [*Singh et al.*, 2010; *Lodhi et al.*, 2013], Greater Noida [*Sharma et al.*, 2014], and Varanasi [*Kumar et al.*, 2012; *Tiwari et al.*, 2013] and have been well calibrated for accuracy in their retrievals. The field of view of the MT is 2.5°, while the full width at half maximum bandwidth at each of the AOD channels is 2.4 ± 0.4 nm. Typical errors in AOD measurements from MT are in the range of 0.02–0.03 [*Morys et al.*, 2001], and the aerosol retrievals were performed from the instantaneous solar flux measurements using the instrument's internal calibration. Furthermore, for minimizing any error in spectral aerosol measurements and the computed parameters, the procedure described by *Sharma et al.* [2014] was considered in each MT data set. At each location, three sets of spectral scans were taken at each time under cloudless skies, from which the one that best coincides with the Ångström's formula ($AOD_\lambda = \beta\lambda^{-\alpha}$) and the second-order polynomial fit in the lnAOD versus lnλ was used for the analysis [*Kaskaoutis*
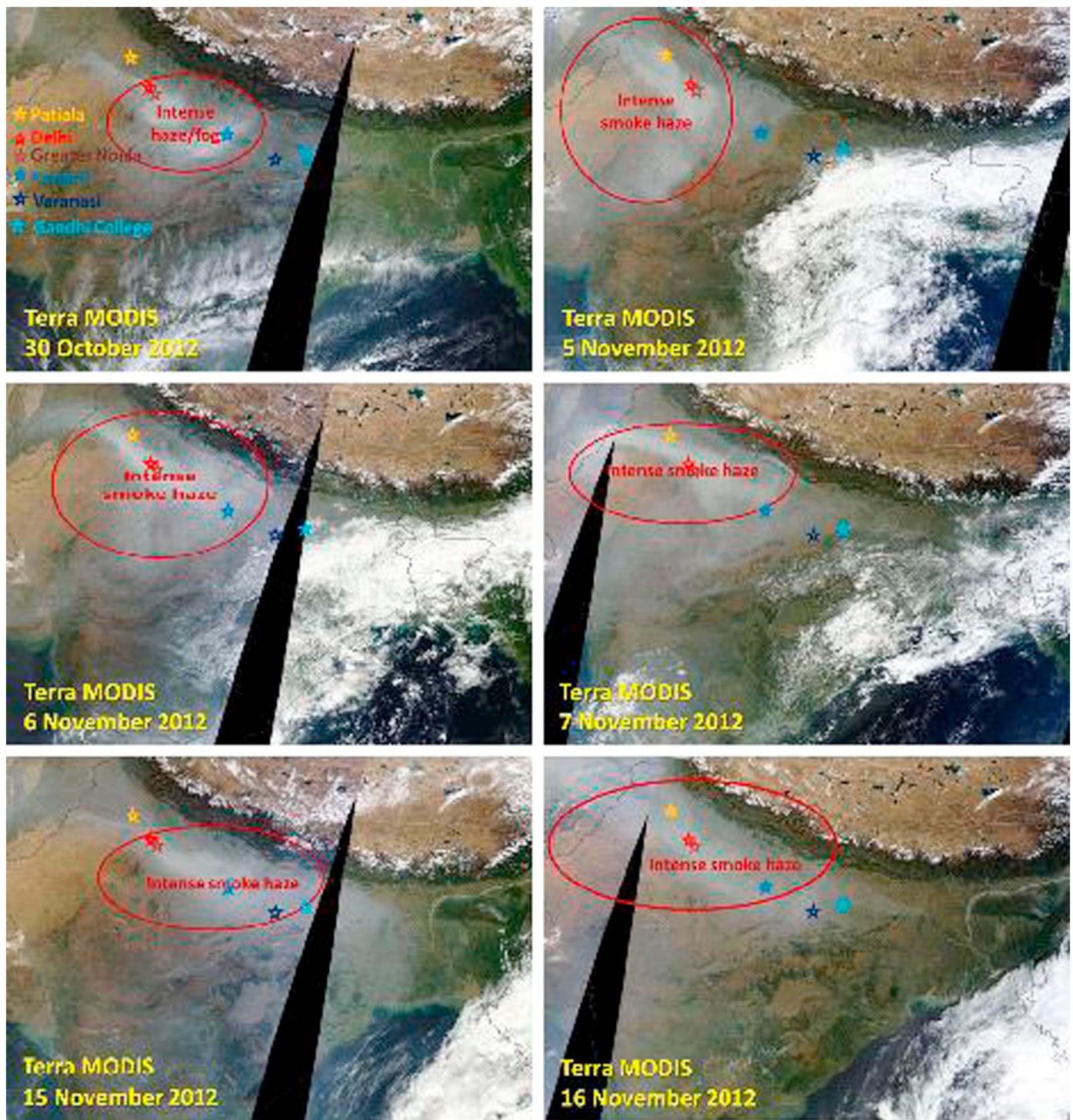
Figure 1. Terra MODIS observations over India during certain days in postmonsoon season 2012 showing thick smoke plumes over IGP and central India.

et al., 2011b; *Sharma et al.*, 2014]. Cases in which the polynomial fit expresses R^2 value below 0.97 were excluded, as well as cases with AOD or Ångström exponent (α) above the daily mean ±2 standard deviation. The latter was taken in order to exclude some few data contaminated by thin (undetectable with the naked eye) cirrus clouds that result in high AOD and low values of α. The Ångström wavelength exponent (α) was obtained from the spectral AODs at each location using the least squares fitting method for the broad spectrum and the Volz method for the narrow bands at shorter and longer wavelengths (see results in Table 2).

Table 2. Aerosol Optical Properties ($AOD_{500\,nm}$, Ångström Exponent at Different Spectral Bands and R_{eff}) Over IGP Sites During the Different Phases of the Burning Period in Postmonsoon 2012[a]

IGP Sites	Aerosol Optical Properties					
Patiala	$AOD_{500\,nm}$	$\alpha_{440-870}$	$\alpha_{380-500}$	$\alpha_{675-870}$		
Preburning (277)	0.55 ± 0.13	0.77 ± 0.17	0.95 ± 0.08	0.62 ± 0.26		
Early burning (246)	0.66 ± 0.36	1.07 ± 0.27	1.07 ± 0.15	1.00 ± 0.38		
Late burning (100)	0.90 ± 0.39	1.03 ± 0.25	0.93 ± 0.21	0.91 ± 0.39		
Postburning (77)	0.51 ± 0.24	0.91 ± 0.18	0.95 ± 0.11	0.66 ± 0.41		
Delhi	$AOD_{500\,nm}$	$\alpha_{340-1020}$	$\alpha_{340-500}$	$\alpha_{870-1020}$		
Preburning (115)	0.60 ± 0.24	0.84 ± 0.17	0.81 ± 0.22	0.98 ± 0.29		
Early burning (78)	0.76 ± 0.26	0.97 ± 0.27	0.87 ± 0.17	0.90 ± 0.35		
Late burning (4)	0.84 ± 0.07	0.97 ± 0.03	0.57 ± 0.03	1.19 ± 0.04		
Postburning (57)	0.59 ± 0.18	0.94 ± 0.11	0.77 ± 0.11	0.79 ± 0.25		
Greater Noida	$AOD_{500\,nm}$	$\alpha_{440-870}$	$\alpha_{380-500}$	$\alpha_{675-870}$		
Preburning (21)	0.64 ± 0.22	1.02 ± 0.18	0.91 ± 0.17	1.12 ± 0.20		
Early burning (16)	1.28 ± 0.61	1.25 ± 0.22	1.04 ± 0.13	1.38 ± 0.31		
Late burning (17)	1.47 ± 0.47	1.21 ± 0.14	0.83 ± 0.14	1.49 ± 0.17		
Postburning (64)	0.84 ± 0.24	1.19 ± 0.17	0.48 ± 0.29	1.37 ± 0.23		
Kanpur	$AOD_{500\,nm}$	$\alpha_{440-870}$	$\alpha_{380-500}$	$\alpha_{675-870}$	$R_{eff}\,f\,(\mu m)$	$R_{eff}\,c\,(\mu m)$
Preburning (126/19)	0.34 ± 0.06	0.92 ± 0.19	0.61 ± 0.31	0.80 ± 0.25	0.148	2.168
Early burning (559/80)	0.87 ± 0.37	1.32 ± 0.15	1.06 ± 0.10	1.31 ± 0.25	0.154	2.277
Late burning (608/81)	1.04 ± 0.39	1.21 ± 0.10	0.80 ± 0.16	1.31 ± 0.16	0.176	2.596
Postburning (486/84)	0.75 ± 0.15	1.19 ± 0.04	0.94 ± 0.09	1.19 ± 0.04	0.155	2.574
Varanasi	$AOD_{500\,nm}$	$\alpha_{440-870}$	$\alpha_{380-500}$	$\alpha_{675-870}$		
Preburning (106)	0.83 ± 0.32	0.81 ± 0.23	1.46 ± 0.22	0.97 ± 0.29		
Early burning (130)	0.82 ± 0.32	0.85 ± 0.19	1.43 ± 0.16	1.29 ± 0.29		
Late burning (270)	1.17 ± 0.31	1.14 ± 0.15	0.92 ± 0.19	1.25 ± 0.29		
Postburning (207)	0.78 ± 0.37	1.17 ± 0.11	1.01 ± 0.19	1.29 ± 0.19		
Gandhi College	$AOD_{500\,nm}$	$\alpha_{440-870}$	$\alpha_{380-500}$	$\alpha_{675-870}$	$R_{eff}\,f\,(\mu m)$	$R_{eff}\,c\,(\mu m)$
Preburning (353/46)	0.90 ± 0.32	1.40 ± 0.08	1.01 ± 0.15	1.53 ± 0.15	0.168	2.510
Early burning (626/65)	0.61 ± 0.20	1.41 ± 0.06	1.11 ± 0.05	1.47 ± 0.11	0.156	2.397
Late burning (324/25)	1.16 ± 0.57	1.35 ± 0.07	0.82 ± 0.14	1.60 ± 0.05	0.183	2.812
Postburning (264/38)	0.81 ± 0.15	1.37 ± 0.06	0.99 ± 0.12	1.50 ± 0.06	0.163	2.695

[a]The total number of spectral scans used for the analysis is shown in parenthesis for each site and burning period. The data for the R_{eff} at the AERONET sites Kanpur and Gandhi College are given after "/."

2.2.2. AERONET

The AERONET retrievals in Kanpur and Gandhi College correspond to cloud-screened and quality-assured (Level 2.0) data following the uncertainties described elsewhere [*Holben et al.*, 1998; *Eck et al.*, 1999; *Dubovik et al.*, 2000; *Smirnov et al.*, 2000; *Singh et al.*, 2004; *Giles et al.*, 2011]. In addition to spectral AOD and Ångström exponent values via direct Sun measurements from CIMEL Sun/sky radiometers (340–1020 nm), the almucantar retrievals (440–870 nm) via the angular distribution and magnitude of sky radiances as well as the measured AOD from direct Sun measurements [*Dubovik et al.*, 2002, 2006] have been also used for the spectral single-scattering albedo (SSA), asymmetry parameter (*g*), and volume size distribution. Common aerosol studies and comparison of the optical and physical properties between Kanpur and Gandhi College can be found elsewhere [*Srivastava et al.*, 2011, 2012; *Kumar et al.*, 2012; *Ramachandran and Kedia*, 2012]. These studies also provide details about the topography, meteorological and atmospheric conditions, aerosol properties, types, and long-range transport.

2.2.3. PM Concentrations

Particulate mass (PM) concentrations were also measured at Patiala University using a GRIMM Aerosol Spectrometer (optical particle counter; Model 1.108; 15 channels) that allows continuous measurements of the size distribution and concentration of airborne particles. Its measuring principle is based on the light scattered by individual particles, incident from a semiconductor laser in a measuring cell. The scattered light pulse from every single particle is counted and the intensity of scattered light signal classified to certain particle size. Scattering induced by particles of various sizes is measured by a photodiode detector, amplified, and finally binned to give the distribution of PM in 15 different grain size classes from 0.3 to 20 μm diameter. The instrument is capable of counting particles from 1 particle l^{-1} of air to 2×10^6 particles l^{-1}, and the lower detectable mass is 0.1 $\mu g m^{-3}$ [*Kharol and Badarinath*, 2006]. The particulate mass concentrations

(PM_{10}, $PM_{2.5}$, and PM_1) were calculated from the particle size distributions using the density factor of 2.8 g cm^{-3} into the instrument's hardware. The PM measurements were taken on a daily basis from 09:00 to 16:00 local standard time (LST) and are integrated for every 5 min before we derive the hourly and daily averaged values.

2.2.4. MODIS Retrievals

Collection 5 (C005) Level 3 (1° × 1°) Terra and Aqua MODIS AOD_{550} values were used over the IGP (22–31°N, 68–89°E) following the dark target approach with lack of data over the arid and desert regions [*Levy et al.*, 2010] in order to reveal the aerosol hot spot areas and spatial gradients during the postmonsoon season of 2012. Several studies [*Tripathi et al.*, 2005; *Jethva et al.*, 2007; *Prasad and Singh*, 2007; *Giles et al.*, 2011; *Shi et al.*, 2011] have shown a satisfactory agreement between MODIS and Kanpur AERONET AODs, since about 72% of the retrievals fall within the expected uncertainty of ±0.05 ± 0.15 × AOD over land [*Levy et al.*, 2010]. MODIS $AOD_{550 nm}$ data were obtained via the Giovanni Online Visualization and Analysis system (http://disc.sci.gsfc.nasa.gov/giovanni). In addition, the MODIS (Terra and Aqua data sets) Fire Mapper product (collection 5, spatial resolution 1 × 1 km) provided by the Fire Information for Resource Management System through the MODIS Adaptive Processing System (https://firms.modaps.eosdis.nasa.gov/firemap/) was used for fire detection over the IGP [*Davies et al.*, 2009]. The detection of fire spots is achieved by a contextual algorithm based on the strong signal of fires in the brightness temperature at infrared (4 and 11 μm) channels [*Giglio et al.*, 2003]. Details about the MODIS fire products are given by *Justice et al.* [2006].

2.2.5. OMI Retrievals

In addition to MODIS, Aura OMI daily aerosol products of Aerosol Index (AI) and NO_2 tropospheric amount in mol/cm^{-2} were used over the IGP during postmonsoon 2012. The data set is Level-2G, Version 003, generated by binning the original pixels from the Level-2 (15 orbits per day, 13 × 24 km spatial resolution) into a 0.25° × 0.25° grid. The OMI algorithm for aerosol detection has been validated via comparisons with ground-based measurements [*Curier et al.*, 2008; *Shaiganfar et al.*, 2011], while comparisons with surface NO_2 show satisfactory agreement suggesting a bias of ±20% [*Irie et al.*, 2008]. AI is suitably used for the detection of soot aerosols and smoke plumes because of their absorbing nature in the UV range, but the main disadvantage is the dependence of its values in the smoke plume altitude [*Eck et al.*, 2001].

2.2.6. CALIPSO Observations

The Cloud-Aerosol Lidar and Infrared Pathfinder Satellite Observation (CALIPSO) flies at an altitude of 705 km with a 98° inclination orbit providing new insight in atmospheric monitoring by observing the vertical profiles of aerosols and clouds [*Omar et al.*, 2009]. The CALIPSO satellite is comprised of three instruments, (i) the Cloud-Aerosol Lidar with Orthogonal Polarization (CALIOP), (ii) the Imaging Infrared Radiometer, and (iii) the Wide Field Camera. The CALIOP Level 1 (version 3.01) attenuated backscatter coefficient at 532 nm (http://www-calipso.larc.nasa.gov/products/) was used in the present study (vertical resolution of 30 m) to reveal the vertical distribution of smoke plumes over northern India during postmonsoon 2012. The CALIPSO calibration and uncertainty as well as the CALIOP data products are discussed in detail by *Powell et al.* [2009] and *Rogers et al.* [2011].

3. Results

3.1. Satellite Monitoring of Crop Residue Burning and Smoke Plumes

Figure 1 presents Terra MODIS true color imagery over northern India on specific days during October–November 2012 revealing a dense smoke/haze cloud that covers the greater part of the IGP. The terrain is nearly obscured below the dense thick plumes, which are shown to be spread from west to central east IGP due to the prevailing northwesterly winds during postmonsoon [*Mishra and Shibata*, 2012]. At times, the dense smoke follows an anticyclonic circulation depending upon the meteorological conditions and affects central India and the northern Arabian Sea [*Badarinath et al.*, 2009a, 2009b]. Satellite images clearly show the smoke cloud along the Indus and Ganges Basins and not so much over the Himalayan foothills and the Tibetan Plateau. However, ground-based measurements [*Bonasoni et al.*, 2010; *Marinoni et al.*, 2010] have shown black carbon (BC) influence over the Himalayas due to transported plumes from the IGP and biomass-burning smoke from Punjab during October and November [*Dumka et al.*, 2010]. Despite the fact that by the end of November the number of fire counts is reduced significantly (see Figure 2a), MODIS observations show high aerosol accumulation over the central eastern IGP, which needs days or weeks to be diluted due to stagnation of air masses, calm winds, and absence of precipitation that do not favor atmospheric ventilation after the termination of the burning season.
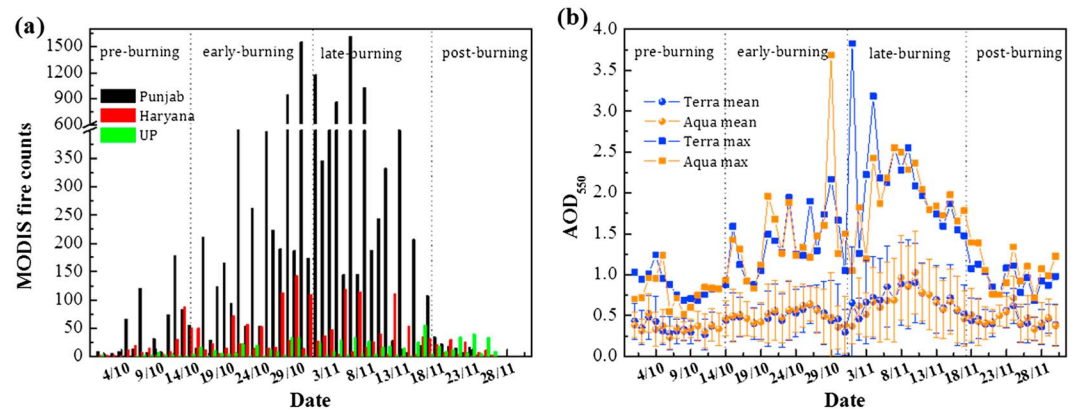
Figure 2. (a) Temporal variation of the MODIS-derived total fire pixels over Punjab, Haryana, and Uttar Pradesh states in the IGP region during the postmonsoon season 2012 and (b) daily variation of the Terra and Aqua MODIS $AOD_{550\,nm}$ (area-averaged and maximum values) over IGP during the same period. The area that has been used for the averages is 22.5°–31.5°N, 74.5°–88.5°E, excluding the pixels over Himalayan range and Tibetan Plateau. The vertical bars express one standard deviation of the area-averaged value on each day.

The analysis of MODIS (Terra and Aqua) active fire counts helps in understanding the possible source regions and their spatiotemporal distribution over the IGP (Punjab, Haryana, and Uttar Pradesh states) during postmonsoon 2012 (Figure 2a). The results show an increase (more than 7 times) in fire counts over Punjab (> 600 on certain days during 28 October to 8 November) compared to other states indicating that paddy crop residue burning is much more common in this region. Fire counts exhibit similar temporal evolution during postmonsoon 2009 [*Mishra and Shibata*, 2012].

The temporal evolution of the spatially averaged MODIS $AOD_{550\,nm}$ over IGP (Figure 2b) provides evidence that fire-related aerosols play an important role since, in general, higher AODs coincide reasonably well with the fire pixels. The correlation coefficient between the daily values of AOD and fire counts reaches to 0.49 for Terra MODIS and 0.32 for Aqua MODIS. It should be noted that the Aqua MODIS fire pixels in Punjab (11,339) are about 10 times higher than those of Terra (1169), while the AOD values over the IGP are also influenced by other sources (urban/industrial aerosols, power plants, and natural particles). On the other hand, the larger number of fire counts does not necessarily mean higher aerosol emissions, since they strongly depend on the severity and the duration of fires as well as the meteorological conditions, dilution, mixing processes, and boundary layer dynamics. Considering the max $AOD_{550\,nm}$ values over the IGP, usually detected over the western parts, the correlation between them and fire pixels gives a coefficient of 0.63 (for Terra) suggesting a significant dependence on biomass burning. Nevertheless, during the preburning period the moderate-to-high AOD (about 0.4 on average) has a significant contribution from dust especially over the western IGP. On the other hand, there is a time lag in the temporal evolution of AOD compared to that of the fire counts, since the aerosol loading remains high during the postburning period; moreover, the highest mean AODs during ~5–12 November seem to be a direct consequence of the peak in fire counts during ~28 October to 8 November. Similar to our results, *Vadrevu et al.* [2011] have observed that the burning activities are well associated with AOD variations over the northwest IGP. The max MODIS AODs are similar in magnitude to those reported over Patiala in October and November 2008 (2.65 and 1.71, respectively) [*Sharma et al.*, 2012], while AODs from agricultural fires above 2.0 were found over Zambia [*Eck et al.*, 2001, 2003], Northeast China and Korea [*Kim et al.*, 2005], and Djougou, Benin [*Pelon et al.*, 2008]. *Eck et al.* [2009] reported AOD values of 0.70–0.98 during the peak biomass-burning season in the boreal forests, while MODIS AODs at the levels of 0.5–0.8 were retrieved over the Mediterranean due to severe Greek wildfires in August 2007 [*Kaskaoutis et al.*, 2011a].

Figure 3 shows the mean spatial distribution of the AI (left) and NO_2 (right) OMI retrievals during the four subperiods over the IGP. The results suggest a larger impact of agricultural burning on both parameters during the late burning period, consistent with MODIS AODs and fire counts (Figure 2). However, AI strongly depends on the smoke plume height with increased values for elevated smoke plumes [*Kahn et al.*, 2008]. Using a combination of AI and CALIOP profiles, *Guan et al.* [2010] found extreme AI > 9 for smoke plumes above 5 km, rendering AI as a surrogate measure for identifying the height of the smoke plumes. In our case,
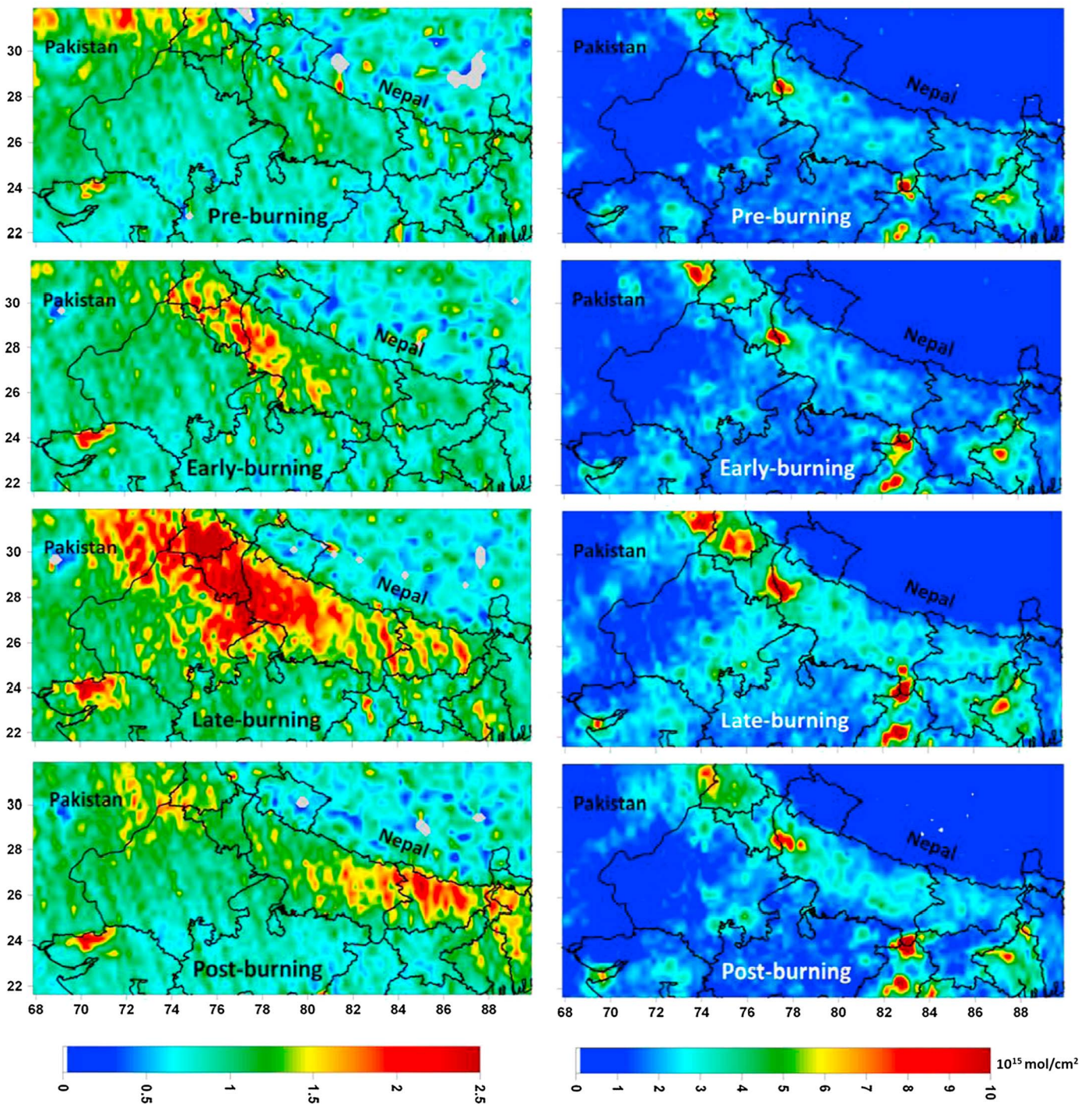
Figure 3. Spatial distribution of (left) Aura OMI-AI and (right) tropospheric NO_2 concentrations over IGP during the four subperiods of the postmonsoon season 2012.

the max AI values approach 2.5, with some extremes of 3–5, suggesting, in general, lower smoke plume altitude. This is also justified via CALIOP profiles (see Figure 5) and is mainly attributed to the lesser potential height of injection that the lower-intensity agricultural fires have compared to the crown forest fires [*Guan et al.*, 2010]. The AI values are similar to those reported for savanna biomass burning in Zambia [*Eck et al.*, 2001, 2003], while AI less than 2.0 was reported over the Himalayas during the peak (April–May) burning season [*Kumar et al.*, 2011; *Vadrevu et al.*, 2012], which was found to correspond to a height of ~2.8 km and to fresh smoke from agricultural fires. It should be noted that AI also depends on the age of the smoke, having
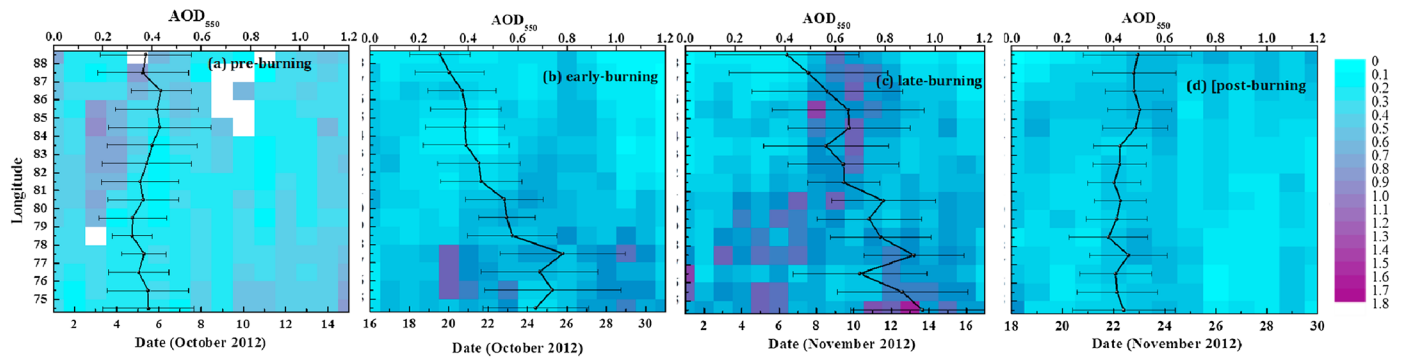
Figure 4. Longitudinal variation of the $AOD_{550\,nm}$ via Terra MODIS observations over IGP region during the four subperiods of the postmonsoon season 2012. The line expresses the averaged longitudinal variation during each period. The vertical bars express one standard deviation from the mean latitudinal-averaged value at each longitude. The area that has been used for the analysis is 22.5°–31.5°N, 74.5°–88.5°E, excluding the pixels over Himalayan range and Tibetan Plateau. White pixels correspond to lack of data.

higher values for fresh smoke aerosols. All of these factors affect AI, which is higher over the western IGP due to a larger abundance of fresh smoke particles, suggesting a strong longitudinal gradient. It is characteristic that by the end of the burning period, the highest AI is detected over eastern IGP indicating accumulation of smoke and anthropogenic aerosols [*Kar et al.*, 2010]. Despite the fact that extra care was taken in excluding AI values at the edges of each orbit path that result in unrealistic high AI (see the stripes), such stripes (mostly raw anomalies) are obvious in the AI spatial distribution; so we avoided any qualitative analysis of the AI.

The impact of the agricultural burning is also evident in the regional air quality and enhanced NO_2 concentrations, which exhibit remarkable spatiotemporal variability, with high values over standard locations associated with urban/industrial centers and/or power plants. Besides this, during the late burning period the moderate-to-high NO_2 values ($3–4 \times 10^{15}$ mol cm^{-2}) cover a more extended area over the IGP as a direct consequence of the biomass-burning emissions. The NO_2 levels during late burning increased about 34–40% on average over the figure's domain compared to the preburning period, reaching up to $8–9 \times 10^{15}$ mol cm^{-2} over rural areas in the western IGP, an amount that is able to attenuate 3–9% the $UV_{300–380\,nm}$ radiation [*Chubarova et al.*, 2012].

3.2. Plume Characteristics, Long-Range Transport, and Affected Areas

Here we discuss the smoke plume characteristics and the altitude of its main transport from the hot spot areas in Punjab to the whole Indian subcontinent and adjoining oceanic regions. The biomass-burning emissions are mainly at the fine and accumulation mode size and can be transported over long distances leading to enhanced aerosol loadings over areas that are mostly clear of aerosols [*Barnaba et al.*, 2011; *Mielonen et al.*, 2013]. Figure 4 shows the longitudinal variation of the latitude-averaged Terra MODIS $AOD_{550\,nm}$ along the IGP during the four subperiods revealing the transport of aerosols and quantifying the west-to-east AOD gradient. The analysis shows higher AOD over the western IGP, especially during the early and late burning periods, which is significantly reduced toward eastern parts, suggesting attenuation of the thickness of the smoke plumes along transport. The high AODs at western pixels (75°–78°E) during 20–23 October and 28 October to 6 November are detected at eastern longitudes (beyond 82°E) after 3–5 days, suggesting that for an average distance of 800 km the smoke plume travels about 4 days. The longitudinal decrease of AOD was satisfactorily simulated by a linear regression and was found to be 98% (86%) on average during the early burning period for Terra (Aqua) and 54% (39%) for Terra (Aqua) during the late burning period. This highlights the strong contribution of agricultural burning in the excess of aerosols over the western IGP during postmonsoon. In contrast, in the postburning period the aerosol loading seems to be higher over the eastern IGP due to accumulation and trapping of aerosols. Although the west-to-east gradients of AOD correspond only to postmonsoon 2012, they are in general agreement with the long-term (2000–2009) gradients observed by *Kaskaoutis et al.* [2011c].

Figure 5 shows the Terra MODIS imagery superimposed with CALIPSO track and CALIOP retrievals during the nighttime of 5 November 2012. The profile of the backscatter coefficient shows large values ($2.5-4.5 \, 10^{-3}$ km^{-1} sr^{-1}) from the surface up to 2.5 km and very low above, since the smoke plumes from agricultural burning are usually trapped within the lower stable boundary layer and are strongly influenced
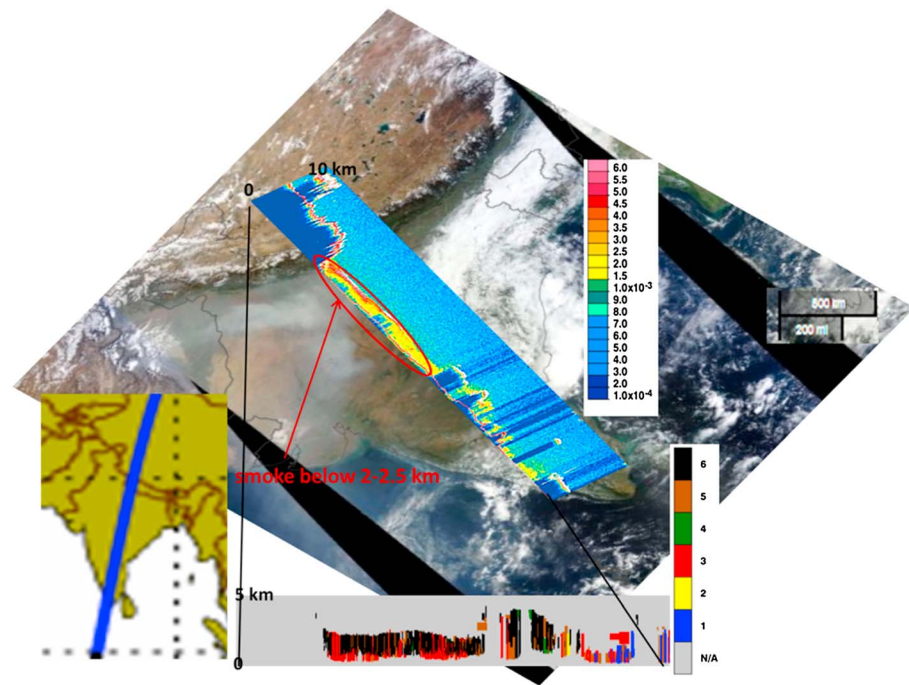
Figure 5. Total attenuated backscatter (km^{-1} sr^{-1}) at 532 nm from nighttime CALIPSO observations on 5 November 2012 (20:31–20:44 UTC, +5:30 LST). The background image corresponds to Terra MODIS on 5 November 2012. The CALIPSO trajectory over India is shown in the inset image, as well as the aerosol subtype (1: clean marine, 2: dust, 3: polluted continental, 4: clean continental, 5: polluted dust, and 6: smoke).

by the static stability of the atmosphere [*Kahn et al.*, 2007]. Similar altitude profiles of the backscatter coefficient were found on other days during the study period, indicating low-level transport of aerosols along the IGP. This is in line with the CALIOP profiles during the postmonsoon 2009 [*Mishra and Shibata*, 2012], when the maximum aerosol loading was found below 1 km, with larger values over the western IGP progressively decreasing toward eastern parts. Modern Era Retrospective-analysis for Research and Applications 2-D data set [*Badarinath et al.*, 2010] over the IGP (0.5° × 0.75° spatial resolution) shows that the boundary layer height varies between ~300 and ~800 m during postmonsoon 2012, suggesting the possibility of smoke plume transport above the boundary layer. The aerosol subtype information [*Omar et al.*, 2009] (inset image) shows strong contribution of smoke aerosols (black), along with continental pollution and dust pollution over the IGP. A similar scenario dominated during the whole burning period, suggesting mixing of biomass burning with dust and anthropogenic emissions over the whole region [*Dey and Tripathi*, 2008]. Comparisons of the CALIOP aerosol subtypes with those reported by AERONET have shown a satisfactory agreement of 70%, with higher accuracy for the coarse particles [*Mielonen et al.*, 2009].

Figure 6 provides insight into the air mass trajectory pathways and traveling heights originating from the biomass-burning hot spot region. In this respect, 5 day forward trajectories were obtained via the HYSPLIT (Hybrid Single-Particle Lagrangian Integrated Trajectory) model [*Draxler and Rolph*, 2003] originating at the matrix (29.5–31.5°N, 74–76°E) located over Punjab. The initial trajectory altitude was fixed at 500 m, since the aerosols are more abundant below 1 km, and the smoke plumes are mostly transported within the lower troposphere (CALIOP profiles). Therefore, the air masses originating from Punjab at this altitude are expected to be heavy smoke laden, since they strongly interact with the planetary boundary layer and the aerosol source. However, this does not prevent aloft air masses from also carrying smoke particles over large distances. The National Center for Environmental Prediction/National Center for Atmospheric Research meteorological field (2.5° × 2.5°) and the vertical wind provided by the model were used for derivation of the forward trajectories, which are plotted against their traveling altitude (colored scale) for each subperiod. The height of the smoke injection and the level of the traveling plume are key parameters in aerosol transport models as they mostly determine the distance and the downwind-affected areas [*Kahn et al.*, 2008].
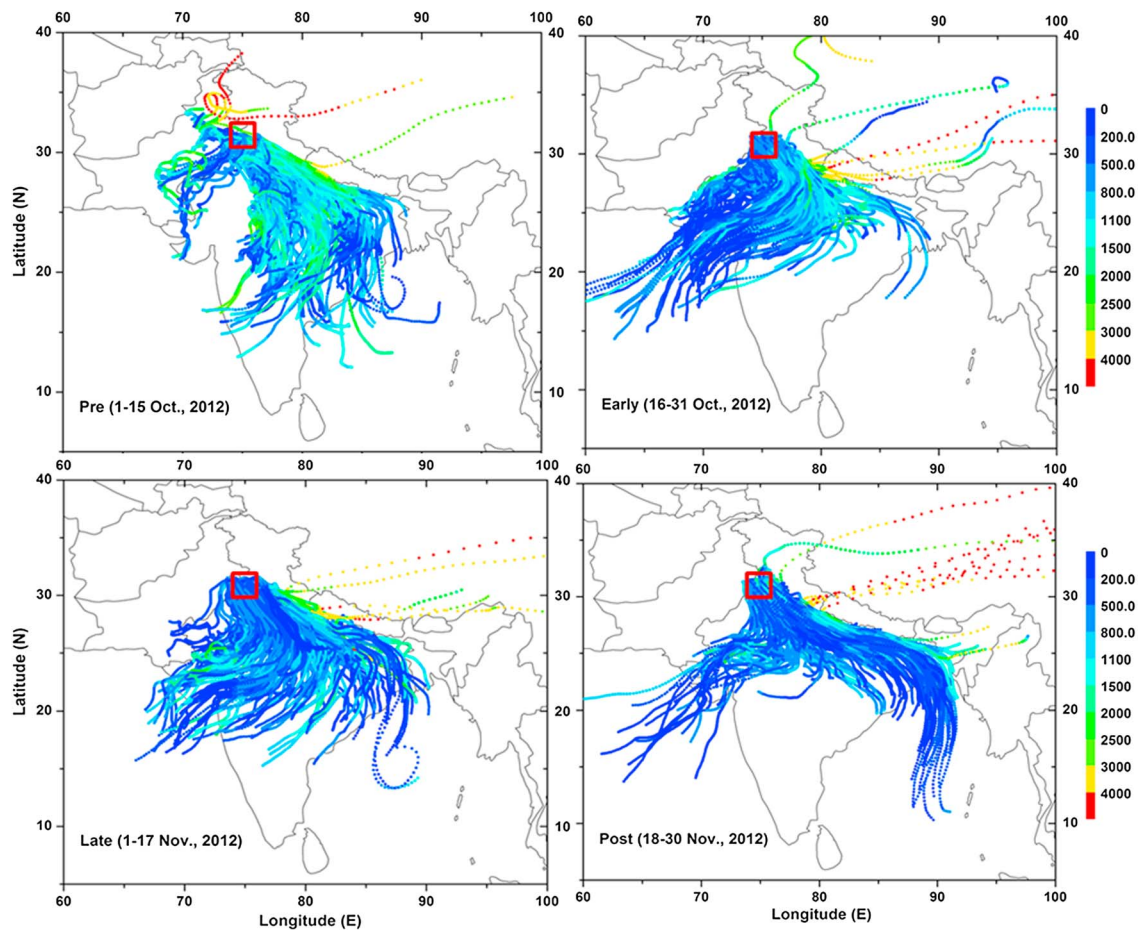
Figure 6. Altitudinal variation of the 5 day forward air mass trajectories starting from Punjab state (matrix: 29.5–31.5°N, 74–76°E, red square) during the four subperiods of the postmonsoon season 2012.

In general, the synoptic meteorology field over the Indian subcontinent during the postmonsoon season is mostly favorable to easterly transport along the IGP [*Kaskaoutis et al.*, 2014], while in some cases it favors the air mass shifting toward the west-southwest affecting central south India [*Badarinath et al.*, 2009a] and the Arabian Sea [*Badarinath et al.*, 2009b]. The analysis shows that in the vast majority of the cases, and above the most affected areas, the traveling height of the air masses is below 500–800 m, which is well within the boundary layer, whereas in some cases, especially during the preburning and early burning periods, the air masses over the IGP may travel above the boundary layer. Smoke-laden air masses originating from Punjab usually travel at higher altitudes (2–2.5 km) over central India, justifying previous results that found elevated smoke-aerosol layers up to 3 km on certain days of October and November [*Badarinath et al.*, 2009a] depending upon the meteorological conditions. The air mass trajectories exhibit some differences proportional to the subperiod, revealing a higher possibility for transported aerosols over the Bay of Bengal during the postburning period. Smoke-laden air masses over the sea regions may affect cloud albedo, microphysical properties, and radiative forcing of marine stratocumulus clouds as earlier observed [*Brioude et al.*, 2009]. On the other hand, the Himalayan-Karakoram-Hindu Kush mountain range is almost not affected by the low-level smoke air masses.

The trajectory-density plot and analysis (Figures 7 and 8) show that the region that is mostly affected by the Punjab-originated smoke air masses is the western IGP, especially during the period 16 October to 17 November, which is the most aerosol-laden (Figures 2 and 3). The eastern IGP is much lesser but also significantly affected, while central India receives smoke air masses mostly during the preburning and late burning periods. The Bay of Bengal and the Arabian Sea are affected the least; however, the influence over the Arabian Sea is higher, justifying the pollution-haze outflow during postmonsoon [*Dey and di Girolamo*, 2010] and the enhanced CO levels [*Badarinath et al.*, 2009b].
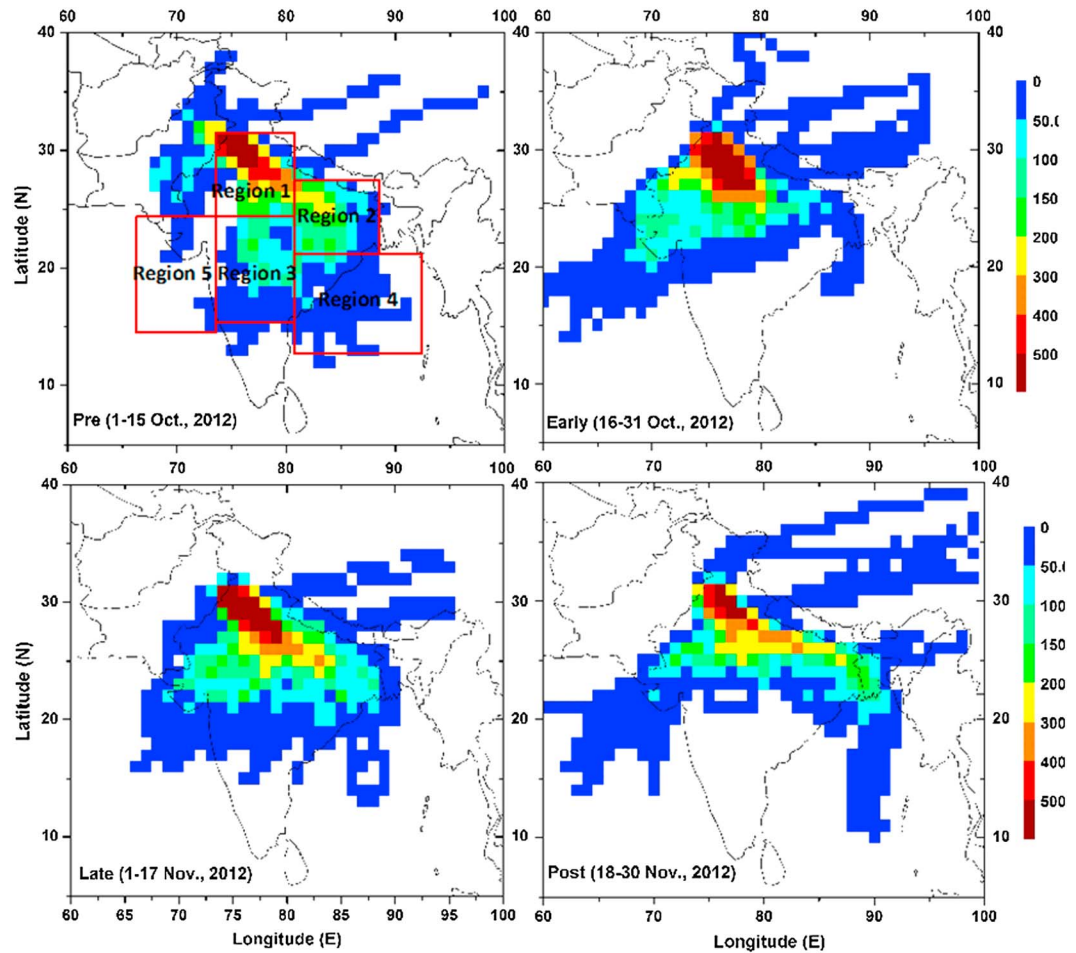
Figure 7. Density plots of the 5 day forward air mass trajectories for each subperiod during the postmonsoon season 2012. (Region 1 (24–31°N, 74–80°E): west IGP, Region 2 (22–27°N, 81–88°E): east IGP, Region 3 (15–23°N, 74–80°E): central India, Region 4 (12–21°N, 81–92°E): east coast and Bay of Bengal, and Region 5 (14–23°N, 66–73°E): west coast and Arabian Sea.)

3.3. Aerosol Properties Over Indo-Gangetic Plains

In this section, we have analyzed PM concentrations at Patiala and the optical properties and modification processes of aerosols over six locations in the IGP during the biomass-burning period. Figures 9a–9c show the
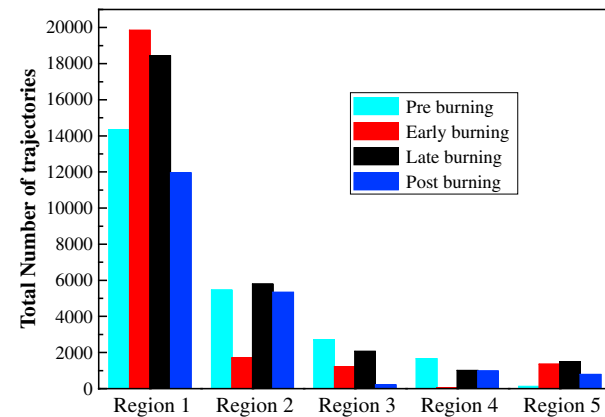

Figure 8. Total number of trajectories at each area defined in Figure 7 for preburning, early burning, late burning, and postburning periods during postmonsoon season 2012.

daytime (09–16 h) variations in PM_{10}, $PM_{2.5}$, and $PM_{1.0}$ concentrations, respectively, measured at Patiala, very close to the aerosol hot spot region. It is shown that the diurnal variability is similar for all of the particle sizes, being more pronounced (morning and afternoon peaks) during the late burning period when the biomass burning is at its highest intensity. Similar diurnal variability, but with lower concentrations, is observed during the early burning period, while during preburning and postburning periods a progressively decreasing diurnal pattern is observed. The diurnal cycle may be explained by the preferable time of agricultural burning, i.e., morning or early afternoon, and by the atmospheric dynamics
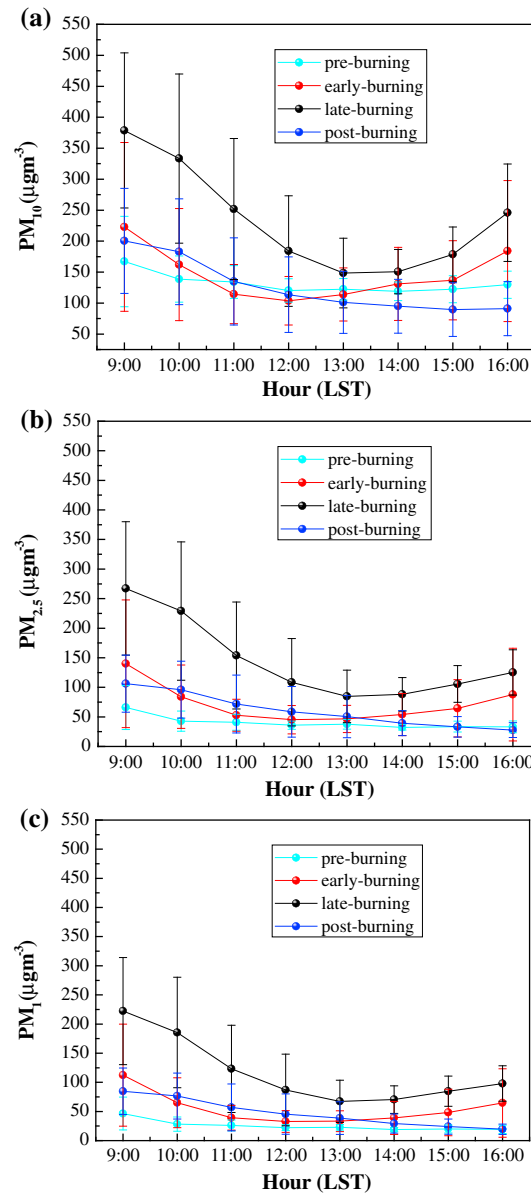
Figure 9. Mean semidiurnal (09:00–16:00 LST) variation of the (a) PM_{10}, (b) $PM_{2.5}$, and (c) $PM_{1.0}$ concentrations at Patiala during the four subperiods of the postmonsoon 2012. The vertical bars correspond to 1 standard deviation of the mean.

forming a deeper boundary layer for aerosol dispersion during noontime. The agricultural burning is very random once the crop is harvested, but normally the farmers avoid the days with high winds. Moreover, it should be noted that the diurnal variation of PM concentrations during the intense burning period is similar to that found for BC aerosols over Patiala [*Sharma et al.*, 2012; *Kharol et al.*, 2012]. Very high PM_{10} concentrations ($> 300\,\mu g\,m^{-3}$, on average, and above $600\,\mu g\,m^{-3}$ on some days) and large fractions of $PM_{2.5}$ and $PM_{1.0}$ (~65% and ~55% of the PM_{10}, respectively) were found during the morning hours of the late burning period, strongly contributing to the formation of haze and limitation of visibility (Figure 10). The daily variation of PM concentrations and their ratios (Figure 10) highlights the large increase in the near-surface aerosol concentrations associated with concurrent enhancement in the fraction of accumulation and fine aerosols during the peak burning period. *Awasthi et al.* [2011] found that $PM_{2.5}$ accounts for ~55%–64% of PM_{10}, while the aerosol load in $PM_{2.5}$ increased by ~80% during the rice crop residue burning compared to the wheat crop residue burning. Furthermore, *Sharma et al.* [2012] found much larger ($150–300\,\mu g\,m^{-3}$) concentrations of $PM_{2.5}$ compared to the coarse ($>PM_{10}$) nonrespirable ($50–180\,\mu g\,m^{-3}$) at Patiala during October–November 2008.

Figure 11 provides the temporal AOD and Ångström α variations at six IGP sites, which can be well explained by the fire counts (Figure 2a) and trajectory analysis (Figures 7 and 8), suggesting intensity of biomass burning and smoke coverage over whole IGP during the 15 October to 15 November period (average increase of 47% and 19% in AOD and α, respectively, compared to the preburning period). The $AOD_{500\,nm}$ over the IGP sites was found to be in the range of ~0.4–~2.4, while in 63% of the cases it was above 0.8. Comparable values for $AOD_{500\,nm}$ (0.81 ± 0.41 and 0.64 ± 0.25) were observed over Patiala in the postmonsoon seasons of 2008 and 2009, respectively

[*Sharma et al.*, 2012], while monthly mean values of 0.57 (October 2009) and 0.74 (November 2009) were reported over Kanpur [*Mishra and Shibata*, 2012]. Increased $AOD_{500\,nm}$ of 0.97 ± 0.56 and 0.76 ± 0.45 was also found over Patiala during the burning seasons of October 2007 and October 2006, respectively [*Sharma et al.*, 2010]. High values (up to 1.2) of $AOD_{550\,nm}$ were observed over Finland due to transported smoke aerosols from Russian agricultural fires [*Arola et al.*, 2007], while *Chubarova et al.* [2012] found extreme maximum $AOD_{500\,nm}$ values of ~6 at west Russian AERONET sites due to severe 2010 wildfires. The temporal variation of α reveals the dominance of the fine aerosols (values above 1.2 during the peak burning), which are comparable to those found for biomass burning in Amazonia and African Savannas [*Reid et al.*, 1999, 2005]. Comparable values (1.31 ± 0.31, October 2007, and 1.10 ± 0.26, October 2006) of α were reported over Patiala during the biomass-burning seasons of previous years [*Sharma et al.*, 2010]. The analysis shows an increase in $AOD_{500\,nm}$ during late burning, followed by early burning and associated with concurrent increase in α (Table 2). The values of α are
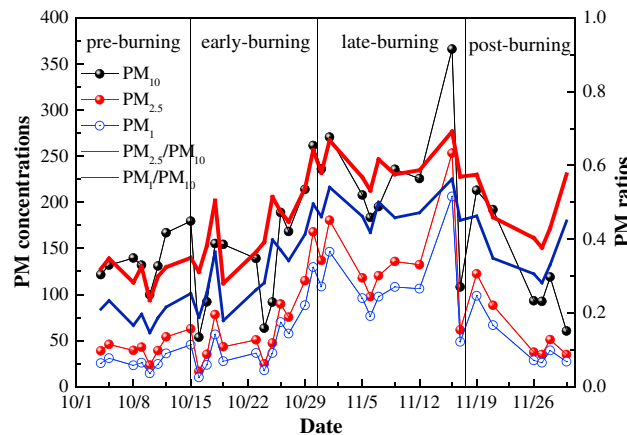
Figure 10. Daily mean variation of the surface PM concentrations as well as the ratios $PM_{2.5}/PM_{10}$ and $PM_{1.0}/PM_{10}$ at Patiala during the postmonsoon 2012.

found to be slightly lower during the late burning period compared to early burning, since the possible coagulation of smoke aerosols and the aging processes lead to formation of larger particles. Moreover, in general, the values of α at longer wavelengths are higher than those at shorter wavelengths during early and late burning periods, leading to a concave type of curve in the $\ln AOD$ versus $\ln\lambda$, indicative of biomass burning [*Eck et al.*, 2001, 2003]. The aerosol properties may differentiate significantly from site to site (Figure 11 and Table 2) since, except smoke, local sources of anthropogenic pollution and soil particles may have a significant contribution to both AOD and α providing a mixing state of

aerosols [*Dey and Tripathi*, 2008] which is more pronounced at the western sites (Patiala, Delhi, and Greater Noida) due to higher dust contribution (closer to the Thar desert).

The Ångström exponent depends on several parameters, such as the refractive index, aerosol size distribution, effective radius, fine-to-coarse-mode fraction, and the wavelength range used for its determination [*Eck et al.*, 1999; *Reid et al.*, 1999]. Figure 12 shows the correlation between $AOD_{500 nm}$ and α at the six IGP locations, suggesting atmospheric characteristics of regions strongly affected by biomass-burning aerosols. Similar scatterplots were observed in South Africa and Amazonia during the dry burning season [*Reid et al.*, 1999; *Eck et al.*, 2003]. The large (>1.0) values of AOD are mostly associated with additional aerosol loading due to agricultural crop residue burning ($\alpha > 1.2$). The atmospheric aerosol mixing/modification processes, such as gas-to-particle conversion, growth by aging and humidification, and coagulation and long-range transport, alter the aerosol properties along the IGP sites. A long tail of decreased α values at lower AODs is shown for the western IGP locations (Patiala, Delhi, and Greater Noida), suggesting more heterogeneous atmospheric conditions and various sources of aerosols, also affected by the arid regions and the Thar desert [*Lodhi et al.*, 2013; *Sharma et al.*, 2014]. In contrast, the easternmost location (Gandhi College) exhibits negligible variability in α values with increasing AOD suggesting homogeneity in sources and a well-mixed atmosphere in which anthropogenic pollution and biomass burning dominate [*Srivastava et al.*, 2012].

Changes in AOD and α values correspond to modification in the aerosol size distribution [$dV(r)/d\ln r$, $\mu m^3/\mu m^2$], shown in Figures 13a and 13b for Kanpur and Gandhi College AERONET sites, respectively. In all cases, the aerosol size distribution shows a bimodal pattern in which the fine-mode possesses a significant or even dominant fraction, characteristic of sites affected by biomass burning, although the Kanpur cases correspond mostly to the urban aerosol type, with significant fraction of coarse mode [*Dubovik et al.*, 2002]. However, during the late burning period, a pronounced increase in fine mode along with a shift of fine R_{eff} toward larger values (Table 2) is observed at both sites. This corresponds to an overall increase in
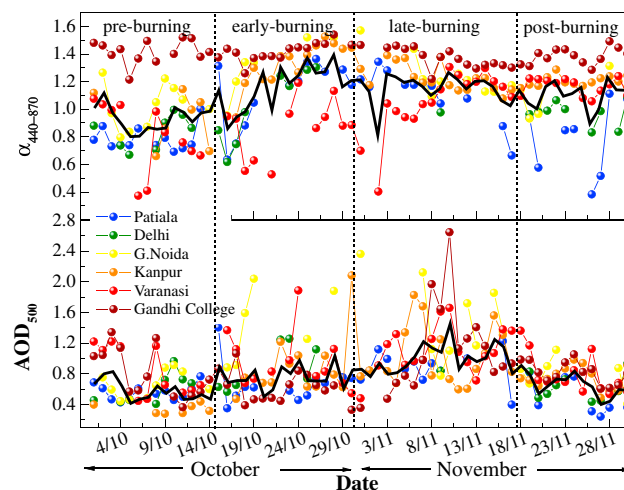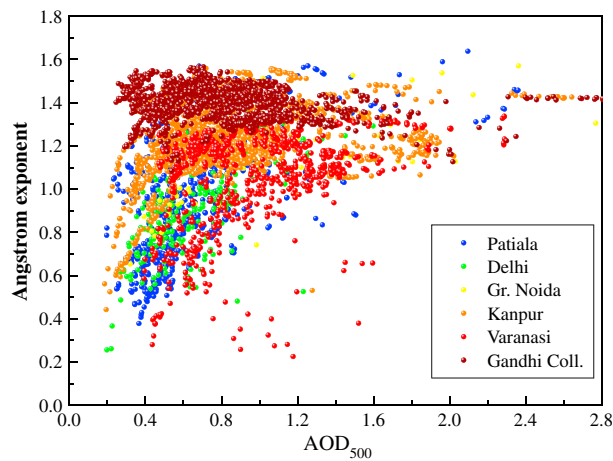

Figure 11. Daily mean variation of the $AOD_{500 nm}$ and Ångström exponent at various locations over IGP during the period 1 October to 30 November 2012. The black lines stand for the mean AOD and α from all sites.

Figure 12. Correlation between $AOD_{500\,nm}$ and Ångström exponent over different locations in IGP region during October–November 2012.

$\alpha_{440-870}$ values; however, the increase in fine-mode radius during the late burning period leads to decrease in $\alpha_{380-500}$ at both sites (Table 2). This is due to coagulation processes that enhance the fine-mode size which are most effective under very turbid environments [*Reid et al.*, 1999]. Similar findings were observed during the severe Russian fires in 2010, where an approximately linear correlation between fine-mode radii and AOD was found but without noticeable changes in the coarse mode [*Chubarova et al.*, 2012]. The influence of crop residue burning seems to be much more intense in the rural environment of Gandhi College (more pronounced increase in fine mode during the late burning period), compared to urban Kanpur, where local activities and traffic resuspend dust enhance the coarse-mode fraction.

Figures 14a and 14b show the spectral variations of SSA and asymmetry parameter (*g*), respectively, over Kanpur and Gandhi College AERONET sites as mean values for each burning period. The SSA spectral values vary from as low as 0.80 to as high as 0.96 between the burning periods and sites, suggesting a strong dependence on many factors, like the type of the biomass, the phase of the burning, aging of emitted smoke, mixing with other aerosol types, OC/EC (organic to elemental carbon) ratios, and meteorological conditions [*Bond and Bergstrom*, 2006; *Eck et al.*, 2003]. SSA values are lower in Kanpur and decrease with wavelength, suggesting more absorbing type of aerosols during early burning, late burning, and postburning periods as this site is closer to the aerosol source, e.g., coal-based power plant, and during burning period strong aerosol mixing is expected [*Prasad et al.*, 2006]. In contrast, the high SSA and spectrally independent values in Kanpur during preburning period are characteristic of well-mixed dust with anthropogenic pollution. Biomass burning enriches the BC concentrations, K^+, and OC/EC ratio [*Kirpa Ram et al.*, 2010], corresponding to enhanced aerosol absorption and AOD. However, the observed SSA values are larger than those reported for fresh smoke from flaming scrub forest fires [*Reid et al.*, 2005] due to mixing and aging processes over IGP. On the other hand, the SSA values over the IGP are similar or slightly lower than those for boreal forest fires, suggesting a significant amount of smoldering combustion resulting in relatively low BC mass fraction [*Eck et al.*, 2009; *Giles et al.*, 2012].

The asymmetry parameter (*g*) defines the angular distribution of scattering and exhibits lower values decreasing with wavelength for smaller and more spherical particles, like soot and carbonaceous aerosols [*Andrews et al.*, 2006]. Both sites exhibit a decreasing tendency of *g* with wavelength with small differences
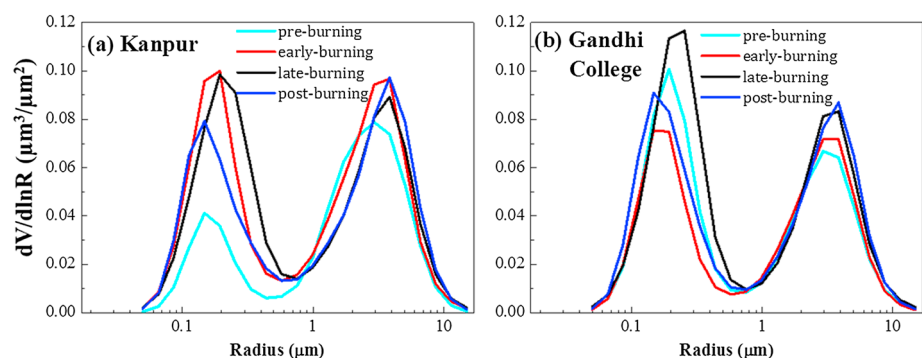

Figure 13. Columnar volume size distribution ($\mu m^3/\mu m^2$) of aerosols over (a) Kanpur and (b) Gandhi College during the different phases of the burning period in postmonsoon 2012.
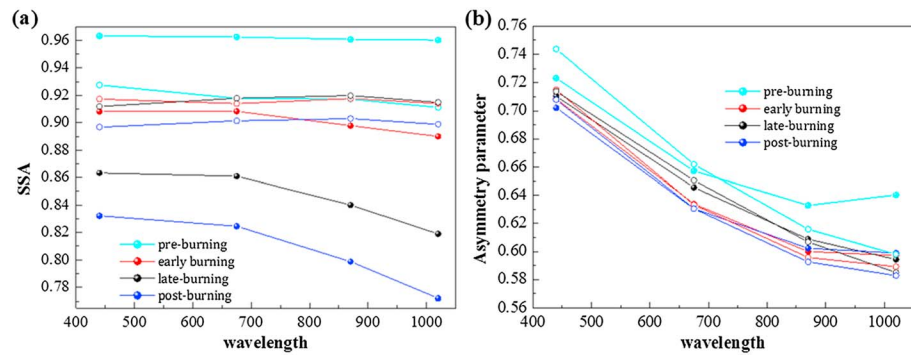
Figure 14. Spectral variation of (a) SSA and (b) asymmetry parameter at Kanpur (filled circles) and Gandhi College (open circles) AERONET stations during the four subperiods of the postmonsoon season 2012. The points for each average are 19 (46), 80 (65), 81 (25), and 84 (38) for preburning, early burning, late burning, and postburning periods, respectively, at Kanpur (Gandhi College).

between the burning periods. Its magnitude of 0.63–0.66 (670 nm) is characteristic for biomass-burning aerosols mixed with anthropogenic and natural particles, while the slight increase in the near-IR region in Kanpur during the preburning period suggests an increased contribution of dust aerosols [*Dubovik et al.*, 2002]. Recently, *Kaskaoutis et al.* [2013] showed that the aerosol episodes ($AOD_{500\,nm} > 0.928$) over Kanpur during the postmonsoon season are the most frequent over the year associated with enhanced presence of biomass-burning aerosols. These modify the aerosol optical and physical properties, increase the radiative forcing, and alter the atmospheric heating rates in a manner that is similar to that observed for the modification in size distribution, spectral SSA, and g.

For studying the aerosol modification processes over the IGP due to the contribution of crop residue burning, we have used a classification scheme [*Gobbi et al.*, 2007], which combines the Ångström exponent ($\alpha_{440-870}$) and its spectral variation ($d\alpha = \alpha_{440-675} - \alpha_{675-870}$) with the radius of fine-mode particles (R_f) and the fine-mode fraction (η) as the grid parameters in grouped AOD. Further details about the scheme preparation, assumptions, and applications are discussed by *Gobbi et al.* [2007] and *Sinha et al.* [2012]. In general, aging and coagulation processes increase R_f. The increase of AOD with R_f infers the aerosol hydration, while increase in AOD with increasing R_f and decreasing α is attributed to the aging and/or coagulation and the reverse (i.e., increase in AOD with decreasing R_f and increasing α) corresponds to freshly emitted fine aerosols [*Kaskaoutis et al.*, 2011b; *Sinha et al.*, 2012]. This scheme was applied over four IGP locations (Patiala, Kanpur, Varanasi, and Gandhi College) (Figures 15a–15d). Pronounced differences were found between the four locations due to heterogeneity in atmospheric composition, urban and industrial emissions, distance from the burning source, and mixing processes during aerosol transport. However, in all cases, the data scatter reveals that the high AODs are mostly clustering at the fine mode corresponding to large (>1.0) values of α, negative $d\alpha$, and large $\eta > 70\%$ values.

Patiala exhibits the largest variation in the scatter plot (α, $d\alpha$, and AOD) indicating various dominant aerosol types and a significant impact of both fine and coarse-mode particles. For the low AOD cases, the scatter is most and these cases confine to a larger fraction of coarse-mode particles ($\eta < 50\%$) during the preburning period (see Table 2). The results reveal that for increasing AOD, the data points exhibit larger α and η values. The increase in AOD and α is closely related to a decrease in R_f to about 0.12–0.15 μm. This suggests an enhanced presence of fine-mode aerosols, mostly freshly emitted soot particles that affect more the R_f, which can be verified by the much higher BC concentrations over Patiala during the turbid days [*Kharol et al.*, 2012; *Sharma et al.*, 2012]. Over Kanpur, the feature differentiates and is characteristic of polluted urban environments as similar results were observed over Beijing [*Wang et al.*, 2011]. Few data points having $d\alpha > 0$ and $\eta < 50\%$ indicate the influence of transported dust over the site, mainly during the preburning period. The increase in AOD does not seem to affect the $\alpha_{440-870}$ values but enhances significantly the fine-mode fraction (80–90%) leading to larger $\alpha_{675-870}$ (Table 2) and increases the R_f (increase in R_{eff} and decrease in $\alpha_{380-500}$ from the early to late burning period in Table 2). The latter corresponds to the coagulation processes discussed in the size distribution graphs (Figure 13). The scatterplot in Varanasi is more complicated in view of the modification processes under more turbid atmospheres and shows some similarities with specific conditions found in
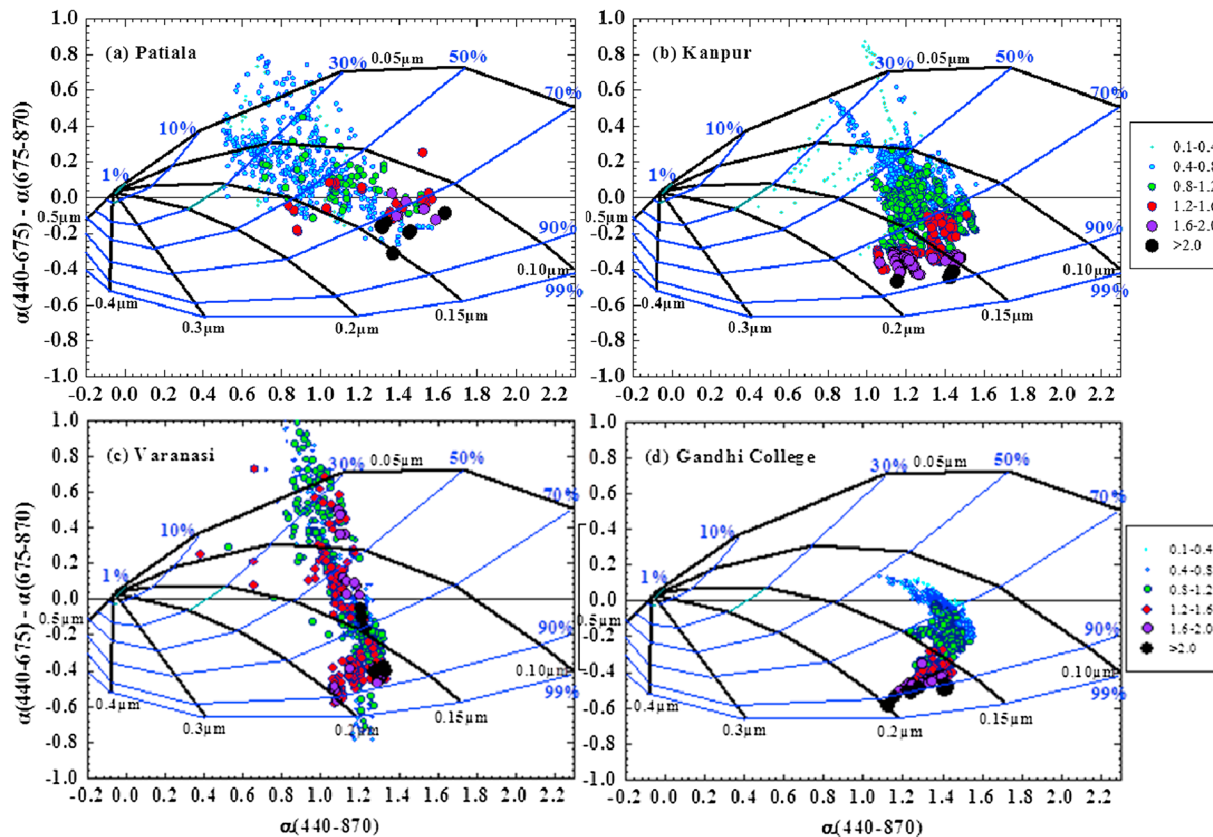
Figure 15. Ångström exponent difference $d\alpha = \alpha(440-675)-\alpha(675-870)$ as a function of the $\alpha_{440-870}$ and $AOD_{500\,nm}$ (color-sized scale) over four IGP sites during postmonsoon 2012, for bimodal lognormal size distribution. The black lines indicate the fixed effective radius (R_f) of the fine mode and the blue lines the fixed fraction (η) of fine mode to the AOD.

Hyderabad during the dry premonsoon season associated with long-range transport of smoke from forest fires in central eastern India [*Sinha et al.*, 2012]. Some of the data points lie outside the classification scheme associated with larger errors in α and $d\alpha$ estimation, but the vast majority of them form a long tail with large variations in $d\alpha$ (−0.6 to 0.8), η (30–90%), and small variations (0.9–1.3) in α. Furthermore, the increase in AOD does not reveal any favorable shift for the other variables, but a small tendency of increasing η is shown corresponding to an enhanced contribution of fine particles. The rather complicated situation can be explained by the high values of AOD and dominance of coarse particles ($\alpha \sim 0.8$) during the preburning period (Table 2). Thus, the increase in AOD may correspond to either enhanced smoke or soil particles depending on the subperiod. Finally, over Gandhi College, the scatterplot reveals the lowest variability among all locations suggesting a well-mixed aerosol and homogeneous atmosphere. The large values of α (1.1–1.5), the large negative $d\alpha$ (below −0.4), and the $\eta = 90\%$ for the high AODs suggest dominance of fine-mode aerosols from fossil fuel and biofuel combustion, manure burning, open fires, etc. Nearly all data points lie in the range 0.12–0.20 μm of R_f, while the concurrent shift toward larger η and higher R_f for increasing AOD corresponds to the coagulation process under a turbid environment strongly dominated by fine-mode aerosols [*Gobbi et al.*, 2007].

4. Conclusions

Any kind of biomass burning is a significant source of carbonaceous aerosols, which play a vital role in atmospheric chemistry, air quality, ecosystems, and human health. Every year during the postmonsoon season (October–November), crop residues are burnt over northwestern India (the state of Punjab). This study examined aerosol properties, smoke plume characteristics, long-range transport, and affected areas during October–November 2012 over the Indo-Gangetic Plains (IGP) region by the synergy of ground-based and satellite observations. MODIS observations revealed a strong west-to-east AOD gradient over the IGP during the peak burning period (15 October to 15 November), since the prevailing northwesterly winds

facilitate the spreading of smoke plumes along the IGP. CALIOP profiles revealed that the smoke plumes were usually transported within the boundary layer and below 2–2.5 km, while the regions that were mostly affected were the western and eastern IGP. In certain circumstances dense smoke plumes also affected central south India and northeastern parts of the Arabian Sea, while the influence over the Bay of Bengal was found to be much lesser. MODIS and ground-based Sun photometer measurements showed high AODs, reaching above 1.5, that were associated with additional aerosol loading due to biomass burning leading to increase in α values, decrease in SSA, and a shift toward larger fine-mode fraction in the aerosol size distribution. The Ångström exponent (>1.2), aerosol size distribution, SSA (0.86–0.91), OMI-AI (>2.0), and NO_2 concentrations (>5–7×10^{15} mol cm^{-2}) showed typical values for moderately absorbing smoke, also mixed with anthropogenic and natural aerosols, especially at locations in the western IGP. The aerosol modification processes under more turbid atmosphere were further investigated. The results over Patiala showed that increasing in AOD affects more the α values (increasing them) and the fine-mode radii (decrease) and in a lesser extent the fine/coarse ratio (increase). This suggests a shift of the fine-mode size distribution toward larger volume and lower particle size, characteristic of an additional contribution of fresh soot particles. The enhanced contribution of biomass-burning aerosols over Kanpur and Gandhi College, except for the increase in fine-mode fraction resulted in a shift toward larger fine-mode radius due to coagulation of aerosols under a severe turbid environment. These conditions significantly modified the atmospheric gas composition, optical and radiative aerosol characteristics, and, as a result, aerosol radiative forcing and climate implications over northern India. Biomass burning over densely populated and polluted areas is of particular concern since it further contributes to the deterioration of the environment. Further elaboration on the atmospheric processes occurring over the IGP during postmonsoon season could make use of the results presented in this study. The knowledge of the optical properties, smoke plume characteristics, and affected areas of the biomass-burning aerosols in this region is very important for climatic studies, taking also into account the increasing trend of agricultural burning during the last decade.

References

Andreae, M. O., and P. Merlet (2001), Emission of trace gases and aerosols from biomass burning, *Global Biogeochem. Cycles*, *15*, 955–966, doi:10.1029/2000GB001382.

Andrews, E., et al. (2006), Comparison of methods for deriving aerosol asymmetry parameter, *J. Geophys. Res.*, *111*, D05S04, doi:10.1029/2004JD005734.

Arola, A., A. Lindfors, A. Natunen, and K. E. J. Lehtinen (2007), A case study on biomass burning aerosols: Effects on aerosol optical properties and surface radiation levels, *Atmos. Chem. Phys.*, *7*, 4257–4266.

Awasthi, A., R. Agarwal, S. K. Mittal, N. Singh, K. Singh, and P. K. Gupta (2011), Study of size and mass distribution of particulate matter due to crop residue burning with seasonal variation in rural area of Punjab, India, *J. Environ. Monit.*, *13*, 1073–1081.

Badarinath, K. V. S., S. K. Kharol, and A. R. Sharma (2009a), Long-range transport of aerosols from agriculture crop residue burning in Indo-Gangetic Plains e a study using LIDAR, ground measurements and satellite data, *J. Atmos. Sol. Terr. Phys.*, *71*, 112–120.

Badarinath, K. V. S., S. K. Kharol, A. R. Sharma, and V. Krishna Prasad (2009b), Analysis of aerosol and carbon monoxide characteristics over Arabian Sea during crop residue burning period in the Indo-Gangetic Plains using multi-satellite remote sensing datasets, *J. Atmos. Sol. Terr. Phys.*, *71*, 1267–1276.

Badarinath, K. V. S., A. R. Sharma, D. G. Kaskaoutis, S. K. Kharol, and H. D. Kambezidis (2010), Solar dimming over the tropical urban region of Hyderabad, India: Effect of increased cloudiness and increased anthropogenic aerosols, *J. Geophys. Res.*, *115*, D21208, doi:10.1029/2009JD013694.

Barnaba, F., F. Angelini, G. Curci, and G. P. Gobbi (2011), An important fingerprint of wildfires on the European aerosol load, *Atmos. Chem. Phys.*, *11*, 10,487–10,501.

Bollasina, M., S. Nigam, and K.-M. Lau (2008), Absorbing aerosols and summer monsoon evolution over South Asia: An observational portrayal, *J. Clim.*, *21*, 3221–3239.

Bonasoni, P., et al. (2010), Atmospheric brown clouds in the Himalayas: First two years of continuous observations at the Nepal Climate Observatory-Pyramid (5079 m), *Atmos. Chem. Phys.*, *10*, 7515–7531.

Bond, T. C., and R. W. Bergstrom (2006), Light absorption by carbonaceous particles: An investigative review, *Aerosol Sci. Technol.*, *40*, 27–67.

Brioude, J., et al. (2009), Effect of biomass burning on marine stratocumulus clouds off the California coast, *Atmos. Chem. Phys.*, *9*, 8841–8856.

Carimichael, G. R., et al. (2009), Asian aerosols: Current and year 2030 distributions and implications to human health and regional climate change, *Environ. Sci. Technol.*, *43*, 5811–5817.

Chubarova, N., Y. Nezval', I. Sviridenkov, A. Smirnov, and I. Slutsker (2012), Smoke aerosol and its radiative effects during extreme fire event over central Russia in summer 2010, *Atmos. Meas. Tech.*, *5*, 557–568.

Curier, R. L., J. P. Veefkind, R. Braak, B. Veihelmann, O. Torres, and G. de Leeuw (2008), Retrieval of aerosol optical properties from OMI radiances using a multiwavelength algorithm: Application to western Europe, *J. Geophys. Res.*, *113*, D17S90, doi:10.1029/2007JD008738.

Davies, D. K., S. Ilavajhala, M. M. Wong, and C. O. Justice (2009), Fire information for resource management system: Archiving and distributing MODIS active fire data, *IEEE Trans. Geosci. Remote. Sens.*, *47*(1), 72–79.

Dey, S., and L. di Girolamo (2010), A climatology of aerosol optical and microphysical properties over the Indian subcontinent from 9 years (2000–2008) of Multiangle Imaging Spectroradiometer (MISR) data, *J. Geophys. Res.*, *115*, D15204, doi:10.1029/2009JD013395.

Dey, S., and S. N. Tripathi (2008), Aerosol direct radiative effects over Kanpur in the Indo-Gangetic basin, northern India: Long-term (2001–2005) observations and implications to regional climate, *J. Geophys. Res.*, *113*, D04212, doi:10.1029/2007JD009029.

Draxler, R. R., and G. D. Rolph (2003), HYSPLIT (Hybrid Single-Particle Lagrangian Integrated Trajectory) model, NOAA Air Resources Laboratory, Silver, Spring, MD. [Available at http://www.arl.noaa. gov/ready/hysplit4.html.]

Dubovik, O., A. Smirnov, B. N. Holben, M. D. King, Y. J. Kaufman, T. F. Eck, and I. Slutsker (2000), Accuracy assessments of aerosol properties retrieved from Aerosol Robotic Network (AERONET) sun and sky radiance measurements, *J. Geophys. Res.*, *105*, 9791–9806, doi:10.1029/2000JD900040.

Dubovik, O., B. N. Holben, T. F. Eck, A. Smirnov, Y. J. Kaufman, M. D. King, D. Tanrè, and I. Slutsker (2002), Variability of absorption and optical properties of key aerosol types observed in worldwide locations, *J. Atmos. Sci.*, *59*, 590–608.

Dubovik, O., et al. (2006), Application of spheroid models to account for aerosol particle nonsphericity in remote sensing of desert dust, *J. Geophys. Res.*, *111*, D11208, doi:10.1029/2005JD006619.

Dumka, U. C., et al. (2010), Characteristics of aerosol black carbon mass concentration over a high altitude location in the central Himalayas from multi-year measurements, *Atmos. Res.*, *96*, 510–521.

Eck, T. F., B. N. Holben, J. S. Reid, O. Dubovik, A. Smirnov, N. T. O'Neill, I. Slutsker, and S. Kinne (1999), Wavelength dependence of the optical depth of biomass burning, urban, and desert dust aerosols, *J. Geophys. Res.*, *104*, 31,333–31,349, doi:10.1029/1999JD900923.

Eck, T. F., B. N. Holben, D. E. Ward, O. Dubovic, J. S. Reid, A. Smirnov, M. M. Mukelabai, N. C. Hsu, N. T. O' Neil, and I. Slutsker (2001), Characterization of the optical properties of biomass-burning aerosols in Zambia during the 1997 ZIBBEE field campaign, *J. Geophys. Res.*, *106*, 3425–3448, doi:10.1029/2000JD900555.

Eck, T. F., et al. (2003), Variability of biomass-burning aerosol optical characteristics in southern Africa during SAFARI 2000 dry season campaign and a comparison of single scattering albedo estimates from radiometric measurements, *J. Geophys. Res.*, *108*(D13), 8477, doi:10.1029/2002JD002321.

Eck, T. F., et al. (2009), Optical properties of boreal region biomass burning aerosols in central Alaska and seasonal variation of aerosol optical depth at an Arctic coastal site, *J. Geophys. Res.*, *114*, D11201, doi:10.1029/2008JD010870.

Feingold, G., H. Jiang, and J. Y. Harrington (2005), On smoke suppression of clouds in Amazonia, *Geophys. Res. Lett.*, *32*, L02804, doi:10.1029/2004GL021369.

Food and Agriculture Organization (2009), Forest fires and the law—A guide for national drafters based on the fire management voluntary guidelines, FAO LEGISLATIVE STUDY 99, 175 pp., ISBN 978-92-5-106151-0.

Forster, P., et al. (2007), Changes in atmospheric constituents and in radiative forcing, in *Climate Change 2007: The Physical Science Basis. Contribution of Working Group I to the Fourth Assessment Report of the Intergovernmental Panel on Climate Change*, pp. 129–234, Cambridge Univ. Press, Cambridge, U. K., and New York.

Gadde, B., S. Bonnet, C. Menke, and S. Garivait (2009), Air pollutant emissions from rice straw open field burning in India, Thailand and the Philippines, *Environ. Pollut.*, *157*, 1554–1558.

Gautam, R., N. C. Hsu, T. F. Eck, B. N. Holben, S. Janjai, T. Jantarach, S.-C. Tsay, and W. K. Lau (2013), Characterization of aerosols over the Indochina peninsula from satellite-surface observations during biomass burning pre-monsoon season, *Atmos. Environ.*, *78*, 51–59.

Giglio, L., J. Descloitres, C. O. Justice, and Y. Kaufman (2003), An enhanced contextual fire detection algorithm for MODIS, *Remote Sens. Environ.*, *87*, 273–282.

Giles, D. M., et al. (2011), Aerosol properties over the Indo-Gangetic Plain: A 1 mesoscale perspective from the TIGERZ experiment, *J. Geophys. Res.*, *116*, D18203, doi:10.1029/2011JD015809.

Giles, D. M., B. N. Holben, T. F. Eck, A. Sinyuk, A. Smirnov, I. Slutsker, R. R. Dickerson, A. M. Thompson, and J. S. Schafer (2012), An analysis of AERONET aerosol absorption properties and classifications representative of aerosol source regions, *J. Geophys. Res.*, *117*, D17203, doi:10.1029/2012JD018127.

Gobbi, G. P., Y. J. Kaufman, I. Koren, and T. F. Eck (2007), Classification of aerosol properties derived from AERONET direct Sun data, *Atmos. Chem. Phys.*, *7*, 453–458.

Guan, H., R. Esswein, J. Lopez, R. Bergstrom, A. Warnock, M. Follette-Cook, M. Fromm, and L. T. Iraci (2010), A multi-decadal history of biomass burning plume heights identified using aerosol index measurements, *Atmos. Chem. Phys.*, *10*, 6461–6469.

Gustafsson, Ö., M. Krusa, Z. Zencak, R. J. Sheeley, L. Granat, E. Engstrom, P. S. Praveen, P. S. P. Rao, C. Leck, and H. Rhode (2009), Brown clouds over South Asia: Biomass or fossil fuel combustion?, *Science*, *323*, 495–498.

Hodnebrog, Ø., et al. (2012), Impact of forest fires, biogenic emissions and high temperatures on the elevated eastern Mediterranean ozone levels during the hot summer of 2007, *Atmos. Chem. Phys.*, *12*, 8727–8750.

Holben, B. N., T. F. Eck, I. Slutsker, D. Tanré, J. P. Buis, A. Setzer, E. Vermote, J. A. Reagan, and Y. A. Kaufman (1998), AERONET—A federated instrument network and data achieve for aerosol characterization, *Remote Sens. Environ.*, *66*, 1–16.

Irie, H., Y. Kanaya, H. Akimoto, H. Tanimoto, Z. Wang, J. F. Gleason, and E. J. Bucsela (2008), Validation of OMI tropospheric NO_2 column data using MAX-DOAS measurements deep inside the north China plain in June 2006: Mount Tai experiment 2006, *Atmos. Chem. Phys.*, *8*, 6577–6586.

Jethva, H., S. K. Satheesh, and J. Srinivasan (2007), Evaluation of Moderate-Resolution Imaging Spectroradiometer (MODIS) collection 004 (C004) aerosol retrievals at Kanpur, Indo-Gangetic basin, *J. Geophys. Res.*, *112*, D14216, doi:10.1029/2006JD007929.

Justice C., L. Giglio, L. Boschetti, D. Roy, I. Csiszar, J. Morisette, and Y. Kaufman (2006), MODIS fire products—Algorithm technical background document. [Available at http://modis.gsfc.nasa.gov/data/atbd/atbdmod14.pdf.]

Kahn, R. A., W.-H. Li, C. Moroney, D. J. Diner, J. V. Martonchik, and E. Fishbein (2007), Aerosol source plume physical characteristics from space-based multiangle imaging, *J. Geophys. Res.*, *112*, D11205, doi:10.1029/2006JD007647.

Kahn, R. A., Y. Chen, D. L. Nelson, F.-Y. Leung, Q. Li, D. J. Diner, and J. A. Logan (2008), Wildfire smoke injection heights: Two perspectives from space, *Geophys. Res. Lett.*, *35*, L04809. doi:10.1029/2007GL032165.

Kar, J., M. N. Deeter, J. Fishman, Z. Liu, A. Omar, J. K. Creilson, C. R. Trepte, M. A. Vaughan, and D. M. Winker (2010), Wintertime pollution over the eastern Indo-Gangetic Plains as observed from MOPITT, CALIPSO and tropospheric ozone residual data, *Atmos. Chem. Phys.*, *10*, 12,273–12,283.

Kaskaoutis, D. G., S. K. Kharol, N. Sifakis, P. T. Nastos, A. R. Sharma, K. V. S. Badarinath, and H. D. Kambezidis (2011a), Satellite monitoring of the biomass-burning aerosols during the wildfires of August 2007 in Greece: Climate implications, *Atmos. Environ.*, *45*, 716–726.

Kaskaoutis, D. G., S. K. Kharol, P. R. Sinha, R. P. Singh, H. D. Kambezidis, A. R. Sharma, and K. V. S. Badarinath (2011b), Extremely large anthropogenic-aerosol contribution to total aerosol load over the Bay of Bengal during winter season, *Atmos. Chem. Phys.*, *11*, 7097–7117.

Kaskaoutis, D. G., S. K. Kharol, P. R. Sinha, R. P. Singh, K. V. S. Badarinath, W. Mehdi, and M. Sharma (2011c), Contrasting aerosol trends over South Asia during the last decade based on MODIS observations, *Atmos. Meas. Tech. Discuss.*, *4*, 5275–5323.

Kaskaoutis, D. G., P. R. Sinha, V. Vinoj, P. G. Kosmopoulos, S. N. Tripathi, A. Misra, M. Sharma, and R. P. Singh (2013), Aerosol properties and radiative forcing over Kanpur during severe aerosol loading conditions, *Atmos. Environ.*, *79*, 7–19.

Kaskaoutis, D. G., E. E. Houssos, D. Goto, A. Bartzokas, P. T. Nastos, P. R. Sinha, S. K. Kharol, P. G. Kosmopoulos, R. P. Singh, and T. Takemura (2014), Synoptic weather conditions and aerosol episodes over Indo-Gangetic Plains, India, *Clim. Dyn.*, doi:10.1007/s00382-014-2055-2, in press.

Kharol, S. K., and K. V. S. Badarinath (2006), Impact of biomass burning on aerosol properties over tropical urban region of Hyderabad, India, *Geophys. Res. Lett.*, *33*, L20801, doi:10.1029/2006GL026759.

Kharol, S. K., K. V. S. Badarinath, A. R. Sharma, D. V. Mahalakshmi, D. Singh, and K. P. Vadrevu (2012), Black carbon aerosol variations over Patiala city, Punjab, India—A study during agriculture crop residue burning period using ground measurements and satellite data, *J. Atmos. Sol. Terr. Phys.*, *84–85*, 45–51.

Kim, S. W., A. Jefferson, S.-C. Yoon, E. G. Dutton, A. J. Ogren, F. P. J. Valero, J. Kim, and B. N. Holben (2005), Comparisons of aerosol optical depth and surface shortwave irradiance and their effect on the aerosol surface radiative forcing estimation, *J. Geophys. Res.*, *110*, D07204, doi:10.1029/2004JD004989.

Koch, D., and A. D. Del Genio (2010), Black carbon semi-direct effects on cloud cover: Review and synthesis, *Atmos. Chem. Phys.*, *10*, 7685–7696.

Kontoes, H., N. Sifakis, and I. Keramitsoglou (2009), GMES burn scar mapping kicks into full gear after 2007 wildfires in Greece, Window on GMES: Discover how GMES is turning into reality e success stories, BOSS4GMES (pub.), (issue 3), pp. 64-69, ISSN 2030-5419.

Kumar, R., M. Naja, S. K. Satheesh, N. Ojha, H. Joshi, T. Sarangi, P. Pant, U. C. Dumka, P. Hegde, and S. Venkataramani (2011), Influences of the springtime northern Indian biomass burning over the central Himalayas, *J. Geophys. Res.*, *116*, D19302, doi:10.1029/2010JD015509.

Kumar, S., S. Kumar, A. K. Singh, and R. P. Singh (2012), Seasonal variability of atmospheric aerosol over the north Indian region during 2005–2009, *Adv. Space Res.*, *50*, 1220–1230.

Lawrence, M. G., and J. Lelieveld (2010), Atmospheric pollutant outflow from southern Asia: A review, *Atmos. Chem. Phys.*, *10*, 11,017–11,096.

Levy, R. C., L. A. Remer, R. G. Kleidman, S. Mattoo, C. Ichoku, R. Kahn, and T. F. Eck (2010), Global evaluation of the collection 5 MODIS dark-target aerosol products over land, *Atmos. Chem. Phys.*, *10*, 10,399–10,420.

Lodhi, N. K., S. N. Beegum, S. Singh, and K. Kumar (2013), Aerosol climatology at Delhi in the western Indo-Gangetic Plain: Microphysics, long-term trends, and source strengths, *J. Geophys. Res. Atmos.*, *118*, 1361–1375, doi:10.1002/jgrd.50165.

Marinoni, A., et al. (2010), Aerosol mass and black carbon concentrations, a two year record at NCO-P (5079 m, southern Himalayas), *Atmos. Chem. Phys.*, *10*, 8551–8562.

Mielonen, T., A. Arola, M. Komppula, J. Kukkonen, J. Koskinen, G. de Leeuw, and K. E. J. Lehtinen (2009), Comparison of CALIOP level 2 aerosol subtypes to aerosol types derived from AERONET inversion data, *Geophys. Res. Lett.*, *36*, L18804, doi:10.1029/2009GL039609.

Mielonen, T., V. Aaltonen, H. Lihavainen, A.-P. Hyvärinen, A. Arola, M. Komppula, and R. Kivi (2013), Biomass burning aerosols observed in northern Finland during the 2010 wildfires in Russia, *Atmosphere*, *4*, 17–34.

Mishra, A. K., and T. Shibata (2012), Synergistic analyses of optical and microphysical properties of agricultural crop residue burning aerosols over the Indo-Gangetic basin (IGB), *Atmos. Environ.*, *57*, 205–218.

Morys, M., F. M. Mims III, S. Hagerup, S. E. Anderson, A. Baker, J. Kia, and T. Walkup (2001), Design calibration, and performance of MICROTOPS II handheld ozone monitor and Sun photometer, *J. Geophys. Res.*, *106*, 14,573–14,582, doi:10.1029/2001JD900103.

Nastos, P. T., A. G. Paliatsos, M. B. Anthracopoulos, E. S. Roma, and K. N. Priftis (2010), Outdoor particulate matter and childhood asthma admissions in Athens, Greece: A time-series study, *Environ. Health*, *9*, 45.

Omar, A. H., et al. (2009), The CALIPSO automated aerosol classification and lidar ratio selection algorithm, *J. Atmos. Oceanic Technol.*, *26*, 1994–2014.

Pelon, J., M. Mallet, A. Mariscal, P. Goloub, D. Tanre, B. D. Karam, C. Flamant, J. Haywood, B. Pospichal, and S. Victori (2008), Microlidar observations of biomass burning aerosol over Djougou (Benin) during African monsoon multidisciplinary analysis special observation period 0: Dust and biomass-burning experiment, *J. Geophys. Res.*, *113*, D00C18, doi:10.1029/2008JD009976.

Pinker, R. T., B. Zhan, and E. G. Dutton (2005), Can satellites observe trends in surface solar radiation?, *Science*, *308*, 850–854.

Powell, K. A., C. A. Hostetler, M. A. Vaughan, R. E. Kuehn, W. H. Hunt, K.-P. Lee, C. R. Trepte, R. R. Rogers, S. A. Young, and D. M. Winker (2009), CALIPSO lidar calibration algorithms. Part I: Nighttime 532-nm parallel channel and 532-nm perpendicular channel, *J. Atmos. Oceanic Technol.*, *26*, 2015–2033.

Prasad, A. K., and R. P. Singh (2007), Comparison of MISR-MODIS aerosol optical depth over the Indo-Gangetic basin during the winter and summer seasons (2000–2005), *Remote Sens. Environ.*, *107*, 109–119.

Prasad, A. K., R. P. Singh, and M. Kafatos (2006), Influence of coal based thermal power plants on aerosol optical properties in the Indo-Gangetic basin, *Geophys. Res. Lett.*, *33*, L05805, doi:10.1029/2005GL023801.

Ram, K., M. M. Sarin, and S. N. Tripathi (2010), A 1 year record of carbonaceous aerosols from an urban site in the Indo-Gangetic Plain: Characterization, sources and temporal variability, *J. Geophys. Res.*, *115*, D24313, doi:10.1029/2010JD014188.

Ramachandran, S., and S. Kedia (2012), Radiative effects of aerosols over Indo-Gangetic Plain: Environmental (urban vs. rural) and seasonal variations, *Environ. Sci. Pollut. Res.*, *19*, 2159–2171.

Ramanathan, V., C. Chung, D. Kim, T. Bettge, L. Buja, J. T. Kiehl, W. M. Washington, Q. Fu, D. R. Sikka, and M. Wild (2005), Atmospheric brown clouds: Impacts on South Asian climate and hydrological cycle, *Proc. Natl. Acad. Sci. U.S.A.*, *102*, 5326–5333, doi:10.1073/pnas.0500656102.

Ramanathan, V., M. V. Ramana, G. Roberts, D. Kim, C. Corrigan, C. Chung, and D. Winkler (2007), Warming trends in Asia amplified by brown cloud solar absorption, *Nature*, *448*, 575–578.

Randles, C. A., and V. Ramaswamy (2008), Absorbing aerosols over Asia: A Geophysical Fluid Dynamics Laboratory general circulation model sensitivity study of model response to aerosol optical depth and aerosol absorption, *J. Geophys. Res.*, *113*, D21203, doi:10.1029/2008JD010140.

Reche, C., et al. (2012), Biomass burning contributions to urban aerosols in a coastal Mediterranean City, *Sci. Total Environ.*, *427-428*, 175–190.

Reid, J. S., T. F. Eck, S. A. Christopher, P. V. Hobbs, and B. N. Holben (1999), Use of the Ångström exponent to estimate the variability of optical and physical properties of aging smoke particles in Brazil, *J. Geophys. Res.*, *104*, 27,473–27,489, doi:10.1029/1999JD900833.

Reid, J. S., T. F. Eck, S. A. Christopher, R. Koppmann, O. Dubovik, D. P. Eleuterio, B. N. Holben, E. A. Reid, and J. Zhang (2005), A review of biomass burning emissions part III: Intensive optical properties of biomass burning particles, *Atmos. Chem. Phys.*, *5*, 827–849.

Rogers, R. R., et al. (2011), Assessment of the CALIPSO lidar 532 nm attenuated backscatter calibration using the NASA LaRC airborne high spectral resolution lidar, *Atmos. Chem. Phys.*, *11*, 1295–1311.

Rosenfeld, D. (2000), Suppression of rain and snow by urban air pollution, *Science*, *287*, 1793–1796.

Roy, D. P., Y. Jin, P. E. Lewis, and C. O. Justice (2005), Prototyping a global algorithm for systematic fire affected area mapping using MODIS time series data, *Remote Sens. Environ.*, *97*, 137–162.

Sahai, S., et al. (2007), A study for development of emission factors for trace gases and carbonaceous particulate species from in situ burning of wheat straw in agricultural fields in India, *Atmos. Environ.*, *41*, 9173–9186.

Sarkar, C., V. Kumar, and V. Sinha (2013), Massive emissions of carcinogenic benzenoids from paddy residue burning in north India, *Curr. Sci.*, *104*, 1703–1709.

Shaiganfar, R., S. Beirle, M. Sharma, A. Chauhan, R. P. Singh, and T. Wagner (2011), Estimation of NOx emissions from Delhi using car MAX-DOAS observations and comparison with OMI satellite data, *Atmos. Chem. Phys.*, *11*, 19,179–19,212, doi:10.5194/acpd-11-19179-2011.

Sharma, A. R., S. K. Kharol, K. V. S. Badarinath, and D. Singh (2010), Impact of agriculture crop residue burning on atmospheric aerosol loading—A study over Punjab state, India, *Ann. Geophys.*, *28*, 367–379.

Sharma, D., M. Singh, and D. Singh (2012), Impact of post-harvest biomass burning on aerosol characteristics and radiative forcing over Patiala, north-west region of India, *J. Instit. Eng.*, *8*, 11–24.

Sharma, M., D. G. Kaskaoutis, R. P. Singh, and S. Singh (2014), Seasonal variability of atmospheric aerosol parameters over Greater Noida using ground Sunphotometer observations, *Aerosol Air Qual. Res.*, *14*, 608–622, doi:10.4209/aaqr.2013.06.0219.

Shi, Y., J. Zhang, J. S. Reid, E. J. Hyer, T. F. Eck, B. N. Holben, and R. A. Kahn (2011), A critical examination of spatial biases between MODIS and MISR aerosol products—Application for potential AERONET deployment, *Atmos. Meas. Technol.*, *4*, 2823–2836.

Singh, R. P., S. Dey, S. N. Tripathi, V. Tare, and B. N. Holben (2004), Variability of aerosol parameters over Kanpur, northern India, *J. Geophys. Res.*, *109*, D23206. doi:10.1029/2004JD004966.

Singh, S., K. Soni, T. Bano, R. S. Tanwar, S. Nath, and B. C. Arya (2010), Clear-sky direct aerosol radiative forcing variations over mega-city Delhi, *Ann. Geophys.*, *28*, 1157–1166.

Sinha, P. R., D. G. Kaskaoutis, R. K. Manchanda, and S. Sreenivasan (2012), Characteristics of aerosols over Hyderabad, in southern peninsular India with the use of different techniques, *Ann. Geophys.*, *30*, 1393–1410.

Smirnov, A., B. N. Holben, T. F. Eck, O. Dubovik, and I. Slutsker (2000), Cloud screening and quality control algorithms for the AERONET data base, *Remote Sens. Environ.*, *73*, 337–349.

Srivastava, A. K., S. Tiwari, P. C. S. Devara, D. S. Bisht, M. K. Srivastava, S. N. Tripathi, P. Goloub, and B. N. Holben (2011), Pre-monsoon aerosol characteristics over the Indo-Gangetic basin: Implications to climatic impact, *Ann. Geophys.*, *29*, 789–804.

Srivastava, A. K., S. N. Tripathi, S. Dey, V. P. Kanawade, and S. Tiwari (2012), Inferring aerosol types over the Indo-Gangetic basin from ground based Sunphotometer measurements, *Atmos. Res.*, *109*, 64–75.

Streets, D. G., and K. F. Yarber (2003), Biomass burning in Asia: Annual and seasonal estimates and atmospheric emissions, *Global. Biogeochem. Cycles*, *17*(4), 1099, doi:10.1029/2003GB002040.

Tiwari, S., A. K. Srivastava, and A. K. Singh (2013), Heterogeneity in pre-monsoon aerosol characteristics over the Indo-Gangetic basin, *Atmos. Environ.*, *77*, 738–747.

Tripathi, S. N., S. Dey, A. Chandel, S. Srivastava, R. P. Singh, and B. Holben (2005), Comparison of MODIS and AERONET derived aerosol optical depth over the Ganga basin, India, *Ann. Geophys.*, *23*, 1093–1101.

Tripathi, S. N., A. K. Srivastva, S. Dey, S. K. Satheesh, and K. Krishnamoorthy (2007), The vertical profile of atmospheric heating rate of black carbon aerosols at Kanpur in northern India, *Atmos. Environ.*, *41*, 6909–6915.

Turetsky, M. R., E. S. Kane, J. Harden, R. Ottmar, K. Manies, E. E. Hoy, and E. S. Kasischke (2011), Recent acceleration of biomass burning and carbon losses in Alaskan forests and peatlands, *Nat. Geosci.*, *4*, 27–31.

Vadrevu, K. P., E. Ellicott, K. V. S. Badarinath, and E. Vermote (2011), MODIS derived fire characteristics and aerosol optical depth variations during the agricultural residue burning season, north India, *Environ. Pollut.*, *159*, 1560–1569.

Vadrevu, K. P., E. Ellicott, L. Giglio, K. V. S. Badarinath, E. Vermote, C. Justice, and W. K. M. Lau (2012), Vegetation fires in the Himalayan region—Aerosol load, black carbon emissions and smoke plume heights, *Atmos. Environ.*, *47*, 241–251.

Wang, S., L. Fang, X. Gu, T. Yua, and J. Gao (2011), Comparison of aerosol optical properties from Beijing and Kanpur, *Atmos. Environ.*, *45*, 7406–7414.